Materials and Methods

Tumor specimens. The Jikei University School of Medicine Ethics Review Committee approved the study protocol with informed consent from all patients. A total of 32 ovarian cancer surgical specimens were obtained at the Jikei University Hospitals. Tumors were histologically classified according to the WHO international system and staged according to the International Federation of Gynecology and Obstetrics (25). All of the 32 cases underwent debulking surgery, and the sizes of the residual tumors were <2 cm in all cases. All cases were serous cystadenocarcinomas. There were 25 stage III cases and 7 stage IV cases.

Among the 32 cases, 4 patients with stage IIIc were diagnosed as having achieved a pathologic complete response according to a second look operation after six courses of chemotherapy, including paclitaxel; cancer did not recur in these patients for >1 year. These cases were termed "supersensitive." In addition, we also selected four patients with stage IIIc who showed progressive disease during chemotherapy, including paclitaxel; these cases were termed "refractory." Three of four supersensitive cases completed six courses of paclitaxel (180 mg/m^2)-carboplatin (AUC 5), and one supersensitive case underwent six courses of paclitaxel only due to an allergic reaction to carboplatin in the first course. On the contrary, refractory cases underwent two to four courses of paclitaxel (180 mg/m^2)-carboplatin (AUC 5) and could not completed six courses of paclitaxel-carboplatin due to progression of the disease. These four supersensitive and four refractory specimens were used for RNA extraction, Affymetrix GeneChip analysis (Santa Clara, CA), and real-time reverse transcription-PCR (RT-PCR).

Excluding the cases used for the GeneChip, the residual 24 surgical specimens were used for immunohistochemical analysis.

Establishment of paclitaxel-resistant ovarian cancer cell lines. Using a human serous ovarian cancer cell line, 2008 (provided by Dr. S.B. Howell, Department of Medicine and the Rebecca and John Moores Cancer Center, University of California-San Diego, La Jolla, CA), we developed two kinds of novel clones resistant to paclitaxel after 40 weeks as follows: 2008/PX2 cells were obtained by biweekly medium changes with 800 ng/mL paclitaxel followed by a 2-hour exposure to paclitaxel, where doses of paclitaxel were escalated stepwise to 6,200 ng/mL; 2008/PX24 cells were obtained by biweekly medium changes with chronic exposure to 2 ng/mL paclitaxel, where doses of paclitaxel were escalated stepwise to 29 ng/mL.

The resistances of these original paclitaxel-sensitive clones and newly developed paclitaxel-resistant 2008 clones were evaluated according to established methods: *in vitro* 2-(2-methoxy-4-nitrophenyl)-3-(4-nitrophenyl)-5-(2,4-disulfonyl)-2H-tetrazolium assay (26) and murine model *in vivo* (27). Briefly, for the *in vitro* experiments, a single-cell suspension of 2008, 2008/PX2, or 2008/PX24 in DMEM supplemented with 10% fetal bovine serum was seeded to a 96-well plate at 3,000 cells per well. Then, the cells were treated with a range of concentrations of paclitaxel and cisplatin (carboplatin is a derivative of cisplatin) from 0.00019 to 50 μmol/L with a 2-fold serial dilution. After 4 days of incubation at 37°C in a humidified incubator containing 5% CO_2, 2-(2-methoxy-4-nitrophenyl)-3-(4-nitrophenyl)-5-(2,4-disulfonyl)-2H-tetrazolium reagent (Cell Counting Kit-8, Dojindo Laboratories, Tokyo, Japan) was added to each well, and the plates were further incubated for a few hours at 37°C. Finally, the absorbance at 450 nm was measured, and the antiproliferating activity of each drug was calculated using the formula: $(1 - T / C) \times 100$ (%), where T and C represent the mean difference in absorbance at 450 nm of the cells treated with drugs (T) and that of the untreated control cells (C). The IC_{50} was obtained from three independent experiments (Table 1).

Table 1. *In vitro* sensitivity of ovarian cancer cell lines to paclitaxel and cisplatin

Cell line	IC_{50} for paclitaxel* (ratio)† (nmol/L)	IC_{50} for cisplatin* (ratio)† (μmol/L)
2008	2.2 ± 0.54 (1.0)	0.50 ± 0.14 (1.0)
2008/PX2	200 ± 58 (92)	0.50 ± 0.42 (1.0)
2008/PX24	120 ± 22 (57)	0.24 ± 0.07 (0.48)

*IC_{50} presents mean ± SD obtained from three independent experiments.
†The numbers in parentheses indicate the ratio of IC_{50}.

For *in vivo* experiments, a single-cell suspension of 2008, 2008/PX2, or 2008/PX24 (1×10^7 cells per mouse) was s.c. inoculated into the right flank of five female mice (BALB/c *nu/nu*). The tumor volume was estimated by two-dimensional measurements using the equation: $ab^2 / 2$, where a and b represent tumor length and width, respectively. When the tumor volume reached 200 to 300 mm^3, 40 mg/kg paclitaxel, 80 mg/kg paclitaxel, or vehicle was given i.v. once weekly for 3 weeks (vehicle: 10% Cremophore/0% ethanol/80% saline).

RNA extraction. Cryostat sections containing >80% cancer cells were microdissected and prepared as tumor specimens. Total RNA from

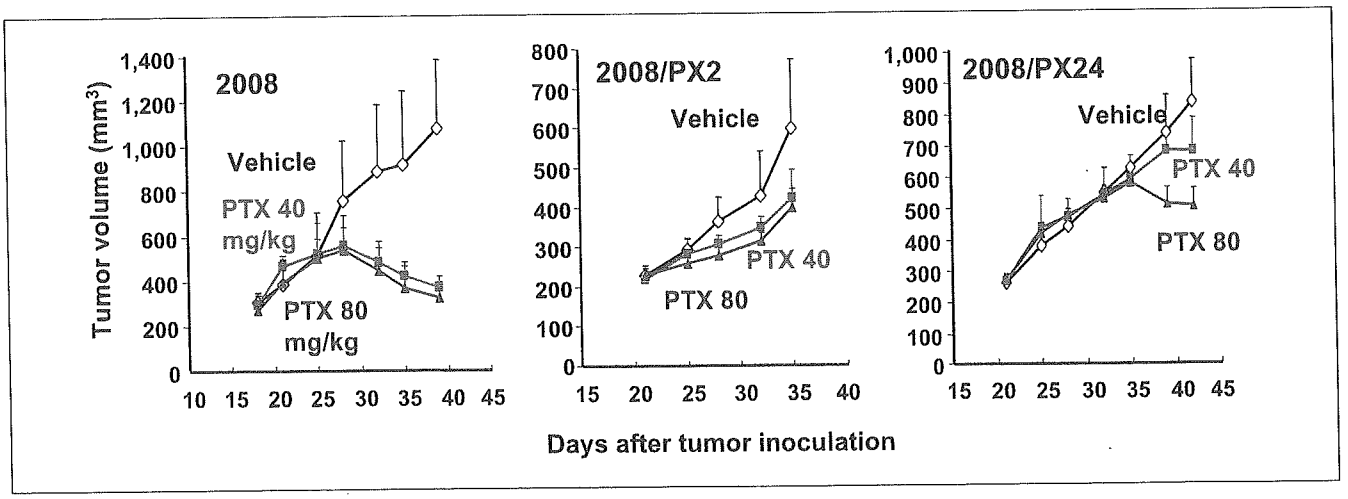

Fig. 1. Murine model to prove chemoresistance of 2008/PX2 and 2008/PX24. A single-cell suspension of 2008, 2008/PX2, or 2008/PX24 (1×10^7 cells per mouse) was s.c. inoculated into the right flank of five female mice (BALB/c *nu/nu*). The tumor volume was estimated by two-dimensional measurements using the equation $ab^2 / 2$, where a and b represent tumor length and width, respectively. When the tumor volume reached 200 to 300 mm^3, 40 mg/kg paclitaxel (*PTX*; ■), 80 mg/kg paclitaxel (▲), or vehicle (◇) was given i.v. once weekly for 3 weeks (vehicle: 10% Cremophore/10% ethanol/80% saline).

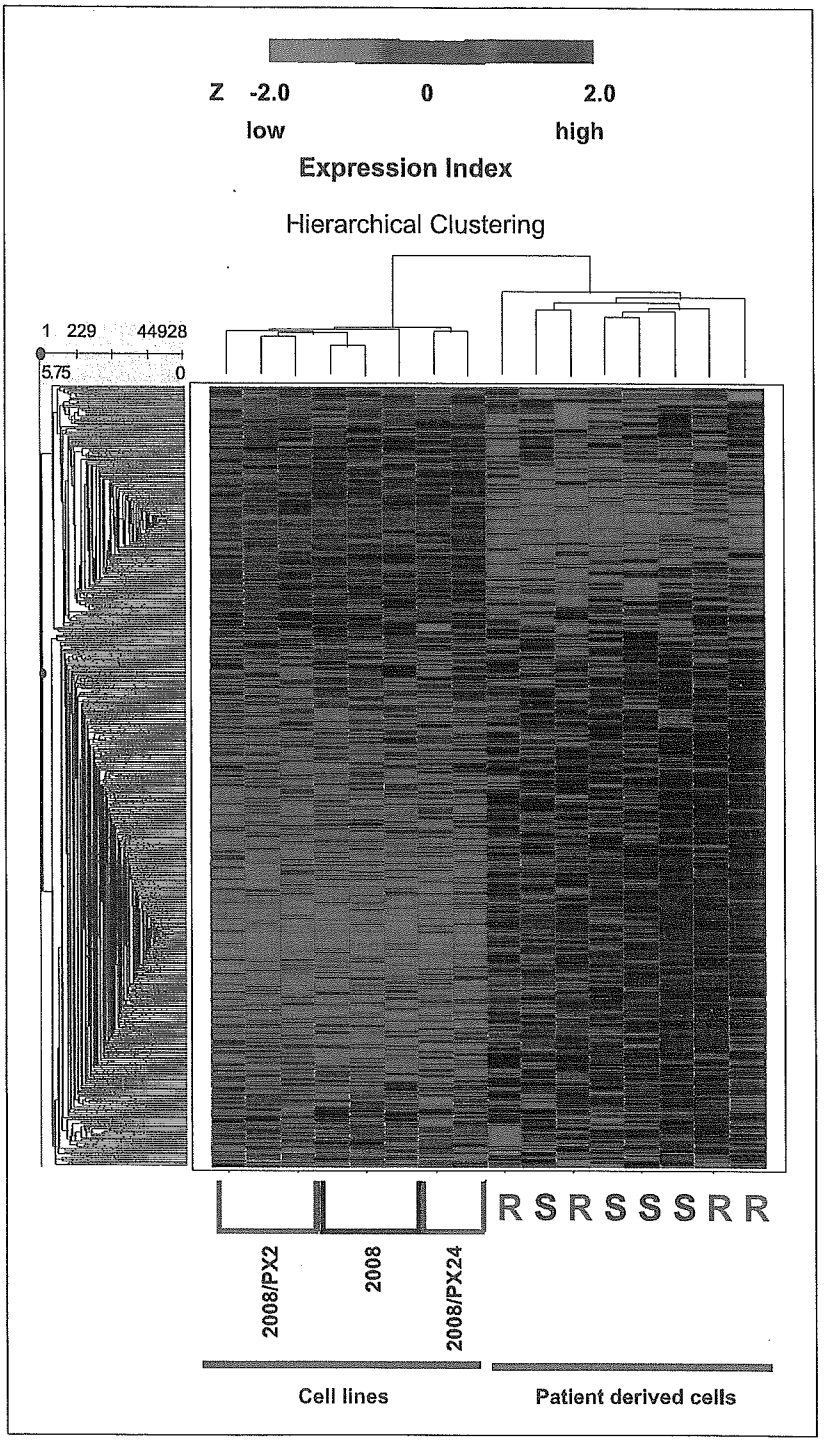

Fig. 2. Gene expression profiles using all data obtained with the GeneChip. Two-dimensional hierarchical clustering was applied to classify all 16 samples of independent extraction of RNA from three kinds of ovarian cancer cell lines (2008, $n = 3$; 2008/PX2, $n = 3$; 2008/PX24, $n = 2$) and 8 surgical tumors (chemosensitive represented as supersensitive, $n = 4$; chemoresistant represented as refractory, $n = 4$) using the 39,000 expressed transcripts. The normalized expression index for each transcript sequence (*rows*) in each sample (*columns*) is indicated by a color code (see expression index bar at the *bottomleft*). R, resistant patient's tumor; S, supersensitive patient's tumor.

ovarian tumors and cell lines were isolated using the hot phenol method (28). Total RNA was isolated from three different cultures of each cell line. We also the scraped ovarian surface epithelium from three menopausal patients with leiomyoma of the uterus who underwent total hysterectomy and bilateral salpingo-oophorectomy with informed consent, and the ovarian surface epithelium was immortalized by SV40 T antigen alone and with SV40 T antigen/human telomerase reverse transcriptase. All six immortalized cell lines are nontumorigenic, and immunocytochemical analysis showed a similar staining pattern to normal ovarian surface epithelium.[8] Total RNA isolated from these immortalized ovarian surface epithelial cells was used as the control for real-time RT-PCR.

Microarray. Human genome-wide gene expression was examined using the Human Genome U133 Array (HG-U133 Set: GeneChip), which contains ~45,000 probe sets, representing >39,000 transcripts derived from ~33,000 well-substantiated human genes (http://www.affymetrix.com/products/arrays/specific/hgu133.affx).

[8] In preparation.

Double-stranded cDNA was synthesized, and the cDNA was subjected to *in vitro* transcription in the presence of biotinylated nucleotide triphosphates. The biotinylated cRNA (10 μg) was hybridized with a probe array for 16 hours at 45°C, and the hybridized biotinylated cRNA was stained with streptavidin-phycoerythrin and then scanned with a Gene Array Scanner. The fluorescence intensity of each probe was quantified using a computer program, GeneChip Analysis Suite 5.0 (Affymetrix). The

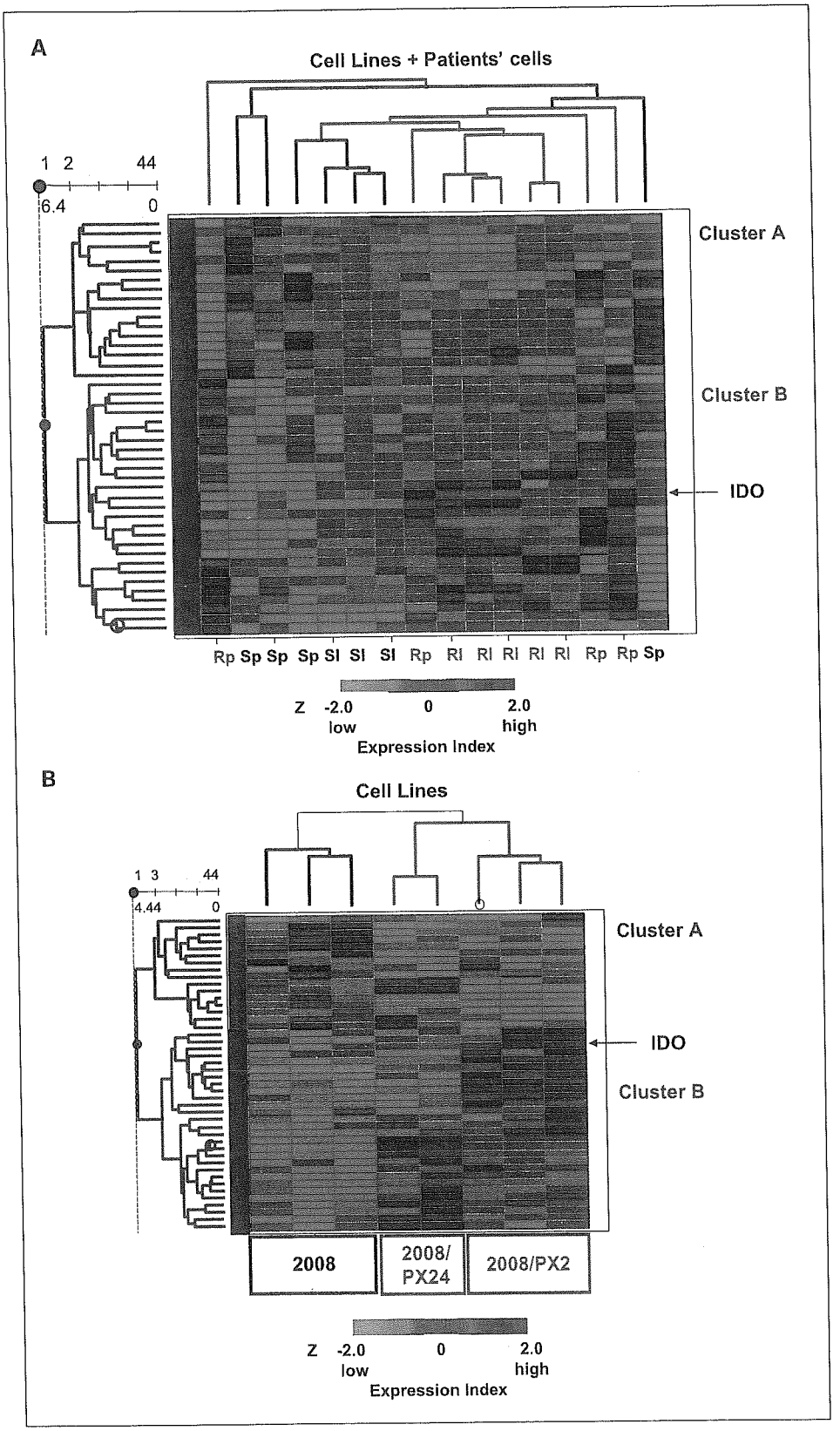

Fig. 3. Gene expression profiles using data of 44 gene expressions that showed significance under permutation tests. *A*, hierarchical clustering of 16 samples of both cell lines and surgical ovarian tumors using normalized data of 44 gene expression profile. Computation clearly separated 44 genes (*row*) into two clusters: cluster A (*blue*), up-regulated in chemosensitive cell lines and supersensitive surgical tumors; cluster B (*pink*), up-regulated in chemoresistant cell lines and resistant surgical tumors. Sp, supersensitive patient's sample; Sl, chemosensitive cell line; Rp, resistant patient's sample; Rl, chemoresistant cell line. *B*, hierarchical clustering of eight samples of cell lines using normalized data of 44 gene expression profile. Computation clearly separated 44 genes (*row*) into two clusters: cluster A (*blue*), up-regulated in chemosensitive cell lines; cluster B (*pink*), up-regulated in chemoresistant cell lines.

expression level of a single RNA was determined as the average fluorescence intensity among the intensities obtained by 11-paired (perfect-matched and single nucleotide-mismatched) probes consisting of 25-mer oligonucleotides. If the intensities of mismatched probes were very high, gene expression was judged to be absent even if a high average fluorescence was obtained with the Microarray Analysis Suite 5.0 program. The data were processed with Affymetrix's default variables, except for scaling (target intensity, 1,000), without normalization procedures to calculate the level of gene expression as the signal.

Quantitative real-time reverse transcription-PCR. Taqman reverse transcription reagents (Applied Biosystems, Foster City, CA) were applied for cDNA synthesis. The SYBR Green reagents kit (Applied Biosystems) was used for quantitative real-time RT-PCR analysis and done according to the manufacturer's recommendations. During RT-PCR, reactions were continuously monitored with an ABI Prism 7700 Sequence Detector (Applied Biosystems). Glyceraldehyde-3-phosphate dehydrogenase messages were used as the internal control. Primers for indoleamine 2,3-dioxygenase (IDO) and glyceraldehyde-3-phosphate dehydrogenase were purchased from Applied Biosystems.

Immunohistochemical analysis. For the immunohistochemical study, formalin-fixed, paraffin-embedded sections were used. Immunostaining was done using the labeled streptavidin-biotin peroxidase complex method with the Ventana auto-immunostaining system (Ventana Japan, Yokoyama, Japan). Murine monoclonal antibody against human IDO (1:1,000; ref. 29) was used. The antigen retrieval procedure was done with a microwave oven in DAKO antigen retrieval solution for 10 minutes at 95°C to efficiently stain the sample. The sections (DAKO Cytomation, Glostrup, Denmark) were developed with 3,3′-diaminobenzidine with 0.3% H_2O_2 and counterstained with hematoxylin. We used surgical specimens that were analyzed with the GeneChip and real-time RT-PCR as positive and negative controls. All of them showed consistent expression of IDO as the results of mRNA expression by real-time RT-PCR. Positive and negative controls were run in parallel for every stain.

Statistics. Hierarchical clustering was analyzed with Spotfire software version 8.0 (Spotfire, Somerville, MA). The *Z*-score (i.e., the SD from the normal mean value of raw data transformed by $\log_2$ in each gene) was used for normalization. First, all genes were included for hierarchical clustering. Second, to adjust the significant level to account for multiple testing in the data sets, permutation tests were applied for gene screening to detect differential expression between chemoresistant and chemosensitive cell lines and patients' tumors. The distribution of maximum t statistics based on 10,000 random permutations was compared with the observed values to determine the P and its 95% confidence interval for each gene using Stata 8.0 (Stata Corp., College Station, TX). Finally, these screened genes were recomputed with hierarchical clustering under sample sets of cell lines and patients' tumors, cell lines alone, and patients' tumors alone.

The association between the stage of cancer and the staining pattern was analyzed with the χ^2 test. Survival curves of the patients were compared using the Kaplan-Meier method. These analyses were done by the log-rank test using Stata 8.0.

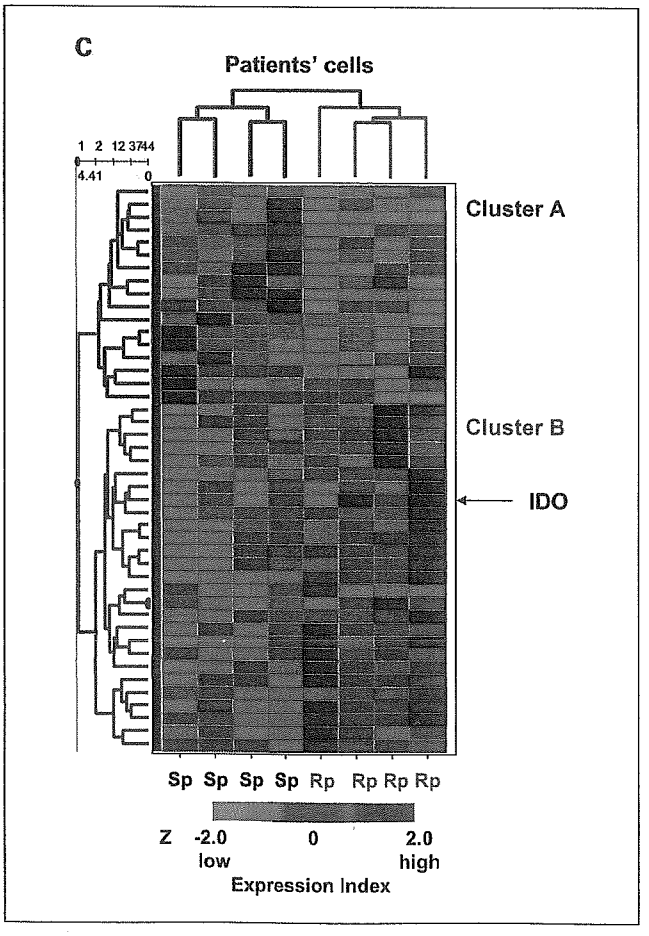

Fig. 3. *Continued. C*, hierarchical clustering of eight samples of surgical tumors using normalized data of 44 gene expression profile. Computation clearly separated 44 genes (*row*) into two clusters: cluster A (*blue*), up-regulated in supersensitive surgical tumors (*green*); cluster B (*pink*), up-regulated in resistant surgical tumors.

Results

Establishment of paclitaxel-resistant ovarian cancer cell lines. After 40 weeks of exposure to paclitaxel, the 2-(2-methoxy-4-nitrophenyl)-3-(4-nitrophenyl)-5-(2,4-disulfonyl)-2H-tetrazolium assay confirmed the development of two cell lines resistant to paclitaxel but still sensitive to cisplatin as follows: the ratio of IC_{50} for paclitaxel between 2008 and 2008/PX2 increased to 92, whereas that for cisplatin remained at 1.0; the ratio of IC_{50} for paclitaxel between 2008 and 2008/PX24 was 57, whereas that for cisplatin was 0.48 (Table 1). Thus, the degree of resistance against paclitaxel was greater in 2008/PX2 than in 2008/PX24, whereas the sensitivity against cisplatin remained the same.

Next, the resistance to paclitaxel of these new cell lines was examined using a murine *in vivo* model and compared with that of the parental cell line, 2008 (Fig. 1). The growth of 2008 in mice was almost completely suppressed by treatment with paclitaxel at 40 and 80 mg/kg (*left*), whereas at the same doses of paclitaxel the growth of 2008/PX2 and 2008/PX24 was only partially suppressed (*middle* and *right*). Thus, the two new cell lines were more resistant to paclitaxel than 2008 both *in vitro* and *in vivo*.

Screening with gene expression profiling. All cell lines (2008, 2008/PX2, and 2008/PX24) and eight surgical tumors from patients (four supersensitive and four refractory) were simultaneously analyzed under hierarchical clustering using all of gene expression data (Fig. 2). Although the cell lines and surgical tumors were clearly differentiated, the nature of the chemosensitivity or chemoresistance was independent of the clusters created by the analysis.

Then, the permutation tests were applied at a cutoff point of 0.05 to screen genes that differentially expressed chemosensitivity and chemoresistance, including both cell lines and surgical tumors. As a result, 44 genes ($P < 0.05$) were selected as candidates associated with chemoresistance or chemosensitivity

Table 2. Permutation analyses of 17 genes

ID	Gene	P*	95% Confidence interval*	R/S ratio both†	R/S ratio cell line‡	R/S ratio patients' tumor§
Permutation analyses of 17 genes down-regulated in both chemoresistant cell lines and resistant tumor specimens						
200963_x_at	*Ribosomal protein L31*	0.0076	0.0060-0.0095	0.83	0.93	0.75
200008_s_at	*GDP dissociation inhibitor 2*	0.0015	0.0008-0.0025	0.68	0.91	0.50
200052_s_at	*Interleukin enhancer binding factor 2, 45 kDa*	0.0080	0.0063-0.0099	0.68	0.96	0.46
200008_s_at	*GDP dissociation inhibitor 2*	0.0086	0.0069-0.0106	0.67	0.89	0.51
200036_s_at	*Ribosomal protein L10a*	0.0326	0.0292-0.0363	0.75	0.75	0.77
201105_at	*Lectin, galactoside binding, soluble, 1 (galectin 1)*	0.0077	0.0061-0.0096	0.53	0.41	0.66
200741_s_at	*Ribosomal protein S27 (metallopanstimulin 1)*	0.0318	0.0284-0.0354	0.78	0.92	0.69
221729_at	*Collagen, type V, α2*	0.0040	0.0029-0.0054	0.37	0.50	0.36
218350_s_at	*Geminin, DNA replication inhibitor*	0.0081	0.0064-0.0101	0.43	0.93	0.28
204031_s_at	*DKFZp564J157 protein*	0.0213	0.0186-0.0243	0.69	0.79	0.60
201524_x_at	*Ubiquitin-conjugating enzyme E2N (UBC13 homologue, yeast)*‖	0.0219	0.0191-0.0250	0.83	0.98	0.67
200934_at	*DEK oncogene (DNA binding)*	0.0295	0.0263-0.0330	0.63	0.75	0.52
200081_s_at	*Ribosomal protein S6*	0.0329	0.0295-0.0366	0.69	0.60	0.80
200081_s_at	*Ribosomal protein S6*	0.0304	0.0271-0.0340	0.69	0.61	0.80
208782_at	*Follistatin-like 1*‖	0.0314	0.0281-0.0350	0.59	0.79	0.42
201054_at	*Heterogeneous nuclear ribonucleoprotein A0*	0.0229	0.0201-0.0260	0.69	0.56	0.86
201518_at	*Chromobox homologue 1 (HP1βhomologue Drosophila)*	0.0390	0.0353-0.0430	0.63	0.88	0.43
Permutation analyses of 17 genes up-regulated in both chemoresistant cell lines and resistant tumor specimens						
205812_s_at	*Sulfotransferase family, cytosolic, 1C, member 2*	0.0016	0.001-0.003	1.58	1.59	1.63
201358_s_at	*Coatomer protein complex, subunit β*	0.0028	0.0019-0.0040	1.66	1.50	1.90
200063_s_at	*Nucleophosmin (nucleolar phosphoprotein B23, numatrin)*	0.0052	0.0039-0.0068	1.24	1.22	1.24
204386_s_at	*Mitochondrial ribosomal protein 63*	0.0111	0.0091-0.0134	1.30	1.21	1.41
224778_s_at	*Homo sapiens, clone IMAGE:5259584, mRNA*	0.0103	0.0084-0.0125	1.56	1.70	1.41
200039_s_at	*Proteasome (prosome, macropain) subunit, βtype, 2*¶	0.0056	0.0042-0.0073	1.45	1.33	1.52
201288_at	*Rho-GDP dissociation inhibitor β*	0.0078	0.0062-0.010	3.13	4.45	2.23
225301_s_at	*Myosin VB*	0.0074	0.0058-0.0093	1.42	1.32	1.53
200055_at	*TAF10 RNA polymerase II, TATA box binding protein-associated factor, 30 kDa*¶	0.0169	0.0145-0.0196	1.55	1.61	1.52
200055_at	*TAF10 RNA polymerase II, TATA box binding protein-associated factor, 30 kDa*	0.0148	0.0125-0.0174	1.59	1.73	1.52
202442_at	*Adaptor-related protein complex 3, σ1 subunit*	0.0022	0.0014-0.0033	1.37	1.43	1.32
208709_s_at	*Nardilysin (N-arginine dibasic convertase)*	0.0409	0.0371-0.0450	1.43	1.20	1.66
201046_s_at	*RAD23 homologue A (Saccharomyces cerevisiae)*	0.0409	0.0371-0.0450	1.57	1.08	2.32
207988_s_at	*Actin-related protein 2/3 complex, subunit 2, 34 kDa*	0.0395	0.0358-0.0435	1.42	1.29	1.54
206445_s_at	*HMT1 hnRNP methyltransferase-like 2 (S. cerevisiae)*	0.0421	0.0382-0.0462	1.44	1.28	1.61
217939_s_at	*Hypothetical protein FLJ20080*	0.0419	0.0381-0.0460	1.41	1.28	1.58
201470_at	*Glutathione S-transferase ω1*	0.0012	0.0006-0.0021	1.45	1.09	1.91
202060_at	*SH2 domain binding protein 1 (tetratricopeptide repeat containing)*	0.0313	0.0280-0.0349	1.75	1.64	1.87
200005_at	*Eukaryotic translation initiation factor 3, subunit 7ζ, 66/67 kDa*	0.0112	0.0092-0.0135	1.66	1.15	2.35
226622_at	*Hypothetical protein FLJ14408*	0.0078	0.0062-0.0097	3.39	1.77	4.85
202090_s_at	*Ubiquinol-cytochrome c reductase (6.4 kDa) subunit*¶	0.0189	0.0163-0.0218	1.33	1.10	1.61
203190_at	*NADH dehydrogenase (ubiquinone) Fe-S protein 8, 23 kDa (NADH-coenzyme Q reductase)*	0.0289	0.0257-0.0324	1.59	1.41	1.74
201077_s_at	*NHP2 nonhistone chromosome protein 2-like 1 (S. cerevisiae)*¶	0.0418	0.0380-0.0459	1.34	1.20	1.43
210029_at	*IDO*b	0.0413	0.0375-0.0454	2.13	1.34	3.20
209374_s_at	*Immunoglobulin heavy constant μ*¶	0.0290	0.0258-0.0325	4.92	2.17	23.07
218261_at	*Adaptor-related protein complex 1, μ2 subunit*	0.0416	0.0378-0.0457	2.03	1.47	2.62
204070_at	*Retinoic acid receptor responder (tazarotene induced) 3*	0.0185	0.0160-0.0213	2.47	1.63	3.40

*P value and 95% confidence interval obtained by permutation *t* tests.
†Mean raw data of chemoresistant cell lines plus resistant patients' tumors/mean raw data of chemosensitive cell lines plus supersensitive patients' tumors.
‡Mean raw data of chemoresistant cell lines/mean raw data of chemosensitive cell lines.
§Mean raw data of resistant patients' tumors/mean raw data of supersensitive patients' tumors.
‖Reduced expression of the gene in chemoresistant cell lines and resistant patients' tumors was confirmed with RT-PCR.
¶Increased expression of the gene in chemoresistant cell lines and resistant patients' tumors was confirmed with RT-PCR.

Table 3. Genes showing reproducible results by real-time RT-PCR

Gene	Function
IDO	Tryptophan degradation
Immunoglobulin heavy constant μ	Immunity
Proteasome	Cleaving peptides in an ATP/ubiquitin – dependent process
Ubiquitin-conjugating enzyme E2N	Ubiquitin-conjugating enzyme
Ubiquinol-cytochrome c reductase	Mitochondrial respiratory chain
TAF10	RNA polymerase II
NHP2 nonhistone chromosome protein 2-like 1	RNA binding protein
Follistatin-like1	Cell growth

and reanalyzed with hierarchical clustering (Fig. 3A). The 44 genes were classified into major two clusters: 17 kinds of genes were down-regulated (Table 2A) representing cluster A in Fig. 3A, whereas 27 genes were up-regulated representing cluster B in Fig. 3A in both chemoresistant cell lines and resistant surgical tumors (Table 2B). Furthermore, we repeated hierarchical clustering restricted to either cell lines alone (Fig. 3B) or surgical tumors alone (Fig. 3C).

Firstly, we assigned priority to 27 genes among 44 genes by either being reported as genes associated with carcinogenesis or being associated with notable pathways. Then, we selected eight genes that showed reproducible results by real-time RT-PCR comparing with the results of GeneChip analysis (Table 3). In particular, IDO was highly and consistently expressed in both chemoresistant cell lines and tumors from refractory patients but not in chemosensitive cell lines and tumors (Fig. 4). This finding was most prominent among these eight genes.

Expression of indoleamine 2,3-dioxygenase protein in pathologic specimens. Expression of IDO protein was further confirmed using pathologic specimens obtained from 24 patients with stage III or IV serous ovarian cancer, excluding samples used for GeneChip analysis. The staining patterns were classified as negative (n = 7; Fig. 5F), sporadic (n = 12; Fig. 5E), focal (n = 3; Fig. 5D), or diffuse (n = 2; Fig. 5C). There was no association between stage of cancer and staining pattern using the χ^2 test.

Indoleamine 2,3-dioxygenase protein expressions and relapse-free survival. First, overall survival was compared between patients with stage III disease (n = 17) and stage IV disease (n = 7) using the log-rank test; no significant difference was noted. Next, Kaplan-Meier survival curves were generated based on the IDO staining pattern (Fig. 6). In contrast to clinical stages, staining patterns of IDO impaired survival (log-rank test, P = 0.0001). All patients classified as negative survived without relapse. The 50% survival of patients classified as sporadic, focal, and diffuse was 41, 17, and 11 months, respectively. We also established a scoring system considering both pattern and intensity, and statistical analysis showed significant differences among every score (data not shown).

Discussion

We screened and identified IDO from 39,000 transcripts as a strong prognostic factor expressed in serous ovarian cancer. Most previous works using gene expression profiling were able to identify a bulk of genes that were highly expressed or suppressed in clinical subgroups of patients, such as those with a differential prognosis (30) or a pathologic type (31). However, fewer studies have shown a single molecule that can be used to clinically distinguish specific subgroups of disease (32, 33). Although microarray technology may be powerful enough to enhance the predictive ability of the prognosis (34), the cost of this technology is still high. In this study, we used microarray technology as a screening tool to identify key molecules associated with chemoresistance in serous ovarian cancer.

Gene expression profiling of novel chemoresistant cell lines was compared with an original chemosensitive cell line to exclude individual differences. However, this approach may

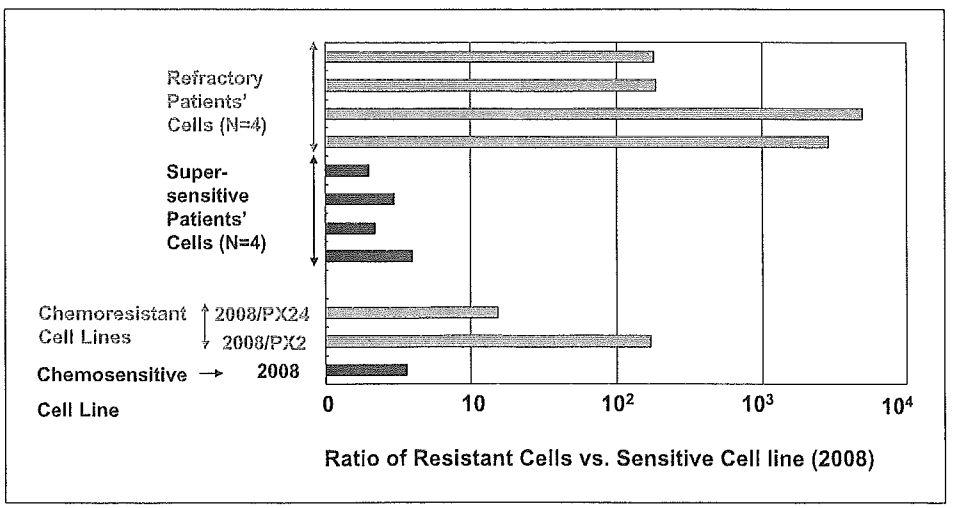

Fig. 4. RNA expression of IDO by real-time RT-PCR. IDO expression in all cell lines (2008, 2008/PX2, and 2008/PX24) and surgical ovarian tumors (supersensitive, n = 4; refractory, n = 4) was measured by real-time RT-PCR. Columns, ratio to a mean of six immortalized ovarian surface epithelial cells for each patient and for each cell line.

pick up genes associated not only with chemoresistant-specific molecules but also with the concurrent changes obtained during the 40 weeks of culture. In contrast, using differential expressions of genes using patients' cells derived from a small sample size, it may be difficult to detect chemoresistant genes, although we carefully selected eight patients who were in the same clinical stage but had a clear contrast between chemosensitive disease and chemoresistant disease in clinical settings. Few previous articles attempted to validate the results obtained from cell lines in patients' cells (35). In this study, a hierarchical clustering of gene expression profiling showed a prominent difference between cell lines and surgically resected patients' tumors but not between chemosensitivity and chemoresistance. Therefore, the permutation tests were applied to abstract chemoresistance-associated genes common to both cell lines and patients' cells. In the selected 27 genes, only 8 were confirmed with real-time RT-PCR, suggesting that the results of the GeneChip and permutation tests cutoff at 0.05 may include some false-positive information. Levels of up-regulation in IDO expression were more prominent in results of real-time RT-PCR than with the GeneChip, which may be due to differences in the methods used to quantify the amounts of RNA expression.

We were able to validate the clinical importance of IDO expression retrospectively using 24 clinical paraffin-embedded specimens, excluding cases used for GeneChip analyses. For patients with advanced serous ovarian cancer, staining patterns of IDO protein expression clearly differentiated between those with a good prognosis and those with a poor prognosis; these prognoses were not predicted by standard clinical staging. This evidence may provide credence to the strategy of starting with genome-wide screening with gene expression profiling using microarray technology, narrowing the number of genes, and ending up with a single gene to link to clinical end points.

IDO, which is a rate-limiting enzyme that catabolizes tryptophan to kynurenine, first attracted a great deal of attention because it could protect against fetal rejection due to immune surveillance (36–38). Recently, tumor cells were also shown to express IDO and to escape the immune surveillance of the host (39, 40) by degrading local tryptophan, which suppresses T cells (41, 42) and natural killer cell proliferation (43, 44). All patients who were negative for IDO survived without relapse, although the duration of survival was impaired depending on the

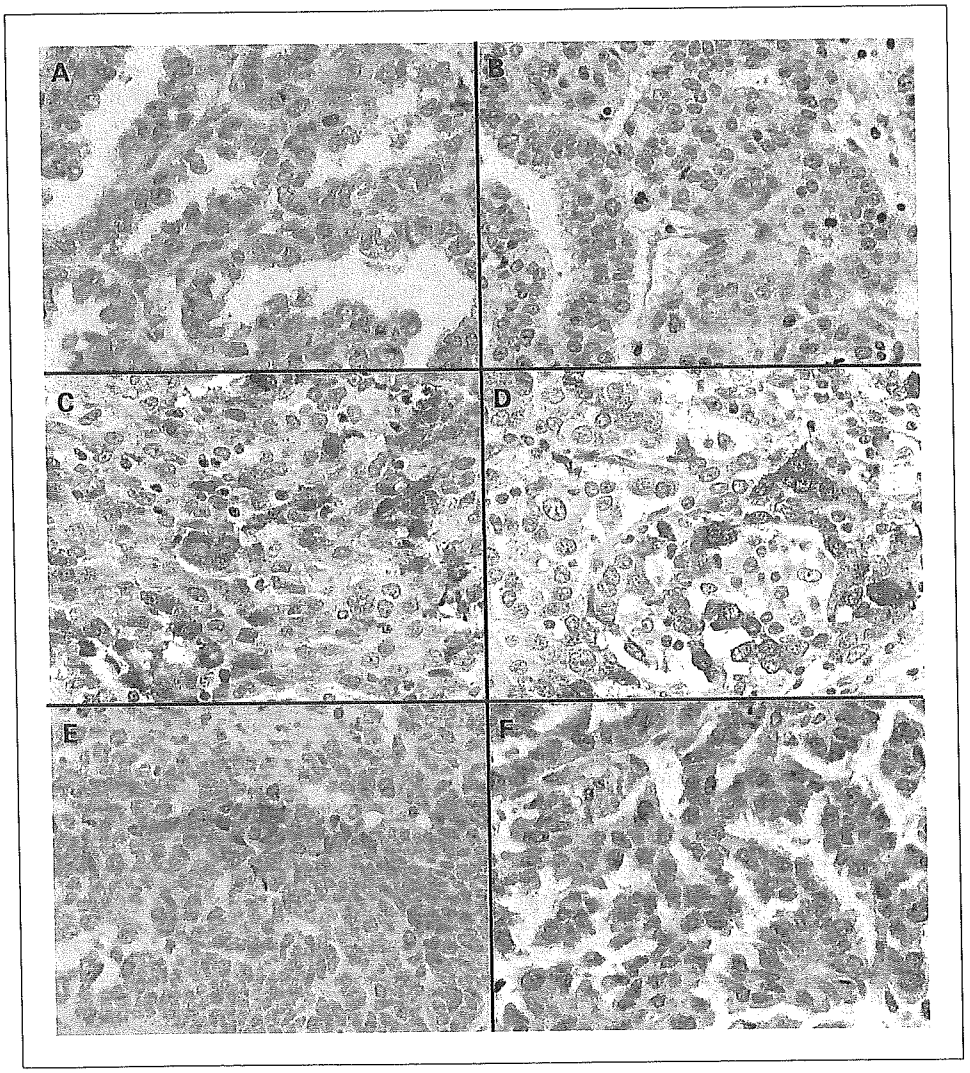

Fig. 5. IDO protein expression in ovarian cancer lesions with immunohistochemical staining. Formalin-fixed, paraffin-embedded sections were stained using the murine monoclonal antibody against human IDO (1:1,000) with the labeled streptavidin-biotin peroxidase complex method and counterstained with hematoxylin. Positive and negative controls of IDO were shown as *A* and *B*, respectively. The staining patterns were classified into diffuse (*C*), focal (*D*) sporadic (*E*), or negative (*F*). Original magnification, ×400.

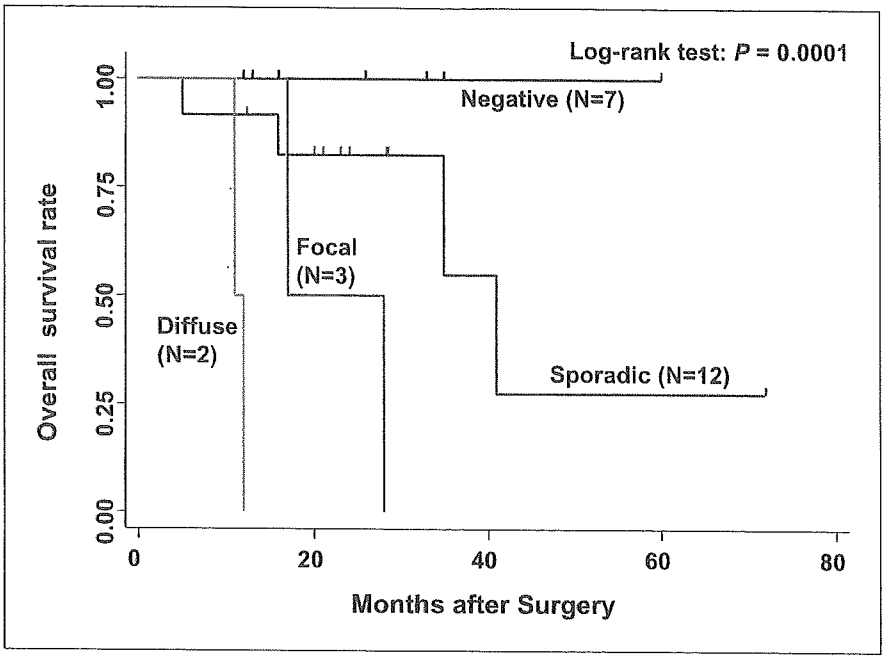

Fig. 6. Patterns of IDO expression in cancerous lesions and overall survival using the Kaplan-Meier method. Excluding cases used for GeneChip analysis, survival data of residual 24 patients were used in this analysis. We used surgical specimens that were analyzed for GeneChip and real-time RT-PCR as the positive and negative controls. All of them showed consistent expression of IDO as the results of mRNA expression by real-time RT-PCR. Patients were restricted to cancer stages III and IV.

pattern of IDO expression. This finding may be explained by the suppression of antitumor immune activities via IDO expression. On the other hand, the recurrence-free survival rate of IDO-positive patients with hepatocellular carcinoma was shown to be significantly higher than that of IDO-negative patients (45). According to their report, IDO-positive cells were identified to be tumor-infiltrating cells, not tumor cells, by immunohistochemical analysis. Although we also examined the staining pattern of tumor-infiltrating cells in the ovarian cancer portion, few cells showed positive staining. On the contrary, positive staining of tumor cells was much more prominent than that of noncancerous cells in all sporadic, focal, and diffuse patterns. Thus, the clinical significance of IDO expression being associated with prognosis in patients with serous-type ovarian cancer may not be universal to all types of cancer.

In this study, greater expression of IDO was confirmed not only in tumors from chemoresistant patients but also in chemoresistant cell lines, suggesting that IDO may affect chemosensitivity through intracellular mechanisms. Recently, IDO expression was shown to be suppressed by nitric oxide, which is known to mediate chemosensitivity in tumor cells via scavenging the production of large quantities of cytosolic superoxide anions (46). On the contrary, hypoxia-induced drug resistance seems to result, in part, from the downstream suppression of endogenous nitric oxide production (47–49). Therefore, the expression of IDO may be a parallel phenomenon to other mechanisms for chemoresistance, such as nitric oxide production, and may not cause chemoresistance directly. Just recently, Muller et al. reported that IDO inhibition cooperated with diverse chemotherapeutic agents to effectively promote the regression of established breast tumors that are refractory to chemotherapy (50). They used MMTV-Neu mice, a well-accepted transgenic mouse model of breast cancer, and showed that combining the IDO inhibitor 1-methyl-DL-tryptophan with paclitaxel resulted in a significant tumor decrease compared with paclitaxel alone (P = 0.0010). Their report supports our data, indicating that IDO is positively associated with paclitaxel resistance and impaired survival. They also indicated that Bin1 loss elevated the signal transducers and activators of transcription 1– and nuclear factor-κB–dependent expression of IDO. Nuclear factor-κB activation suppresses the apoptotic potential of chemotherapeutic agents (51). We speculate that IDO might be positively associated with paclitaxel resistance through the suppression of the apoptotic potential of paclitaxel.

Three of four supersensitive cases underwent paclitaxel-carboplatin, and one case underwent paclitaxel alone due to the hypersensitivity reaction to carboplatin. Moreover, neither 2008/PX2 nor 2008/PX24 showed cross-resistance for cisplatin. Carboplatin is a derivative of cisplatin and is a platinum compound. Using both surgical specimens and cell lines, we purified genes associated with paclitaxel resistance to prevent genes associated with platinum resistance. However, we speculate that IDO not only plays a role in paclitaxel resistance but also has an indirect effect on platinum *in vivo*. The latter speculation is supported by Muller et al. (50). They also showed that 1-methyl-DL-tryptophan with cisplatin also resulted in a significant tumor decrease compared with cisplatin alone. Future study should focus on the functional insights regarding the *IDO* gene for chemoresistance to paclitaxel by gene knockdown, such as the RNA interference technique.

In conclusion, IDO screened with the GeneChip was positively associated with paclitaxel resistance and impaired survival in patients with serous-type ovarian cancer.

Acknowledgments

We thank Mika Endo (Pharmaceutical Research Department 2, Research Division, Chugai Pharmaceutical Co., Ltd.) for assistance with *in vivo* experiments and Misako Arima (Department of Pathology, Jikei University School of Medicine) for technical assistance with immunohistochemistry.

References

1. Partridge EE, Barnes MN. Epithelial ovarian cancer: prevention, diagnosis, and treatment. CA Cancer J Clin 1999;49:297–320.
2. van der Burg ME, van Lent M, Buyse M, et al. The effect of debulking surgery after induction chemotherapy on the prognosis in advanced epithelial ovarian cancer. Gynecological Cancer Cooperative Group of the European Organization for Research and Treatment of Cancer. N Engl J Med 1995;332:629–34.
3. McGuire WP, Hoskins WJ, Brady MF, et al. Cyclophosphamide and cisplatin compared with paclitaxel and cisplatin in patients with stage III and stage IV ovarian cancer. N Engl J Med 1996;334:1–6.
4. Qazi F, McGuire WP. The treatment of epithelial ovarian cancer. CA Cancer J Clin 1995;45:88–101.
5. Agarwal R, Kaye SB. Ovarian cancer: strategies for overcoming resistance to chemotherapy. Nat Rev Cancer 2003;3:502–16.
6. Vasey PA. Resistance to chemotherapy in advanced ovarian cancer: mechanisms and current strategies. Br J Cancer 2003;89:S23–8.
7. Fraser M, Leung BM, Yan X, Dan HC, Cheng JQ, Tsang BK. p53 is a determinant of X-linked inhibitor of apoptosis protein/Akt-mediated chemoresistance in human ovarian cancer cells. Cancer Res 2003;63:7081–8.
8. Tanaka H, Ohshima N, Ikenoya M, Komori K, Katoh F, Hidaka H. HMN-176, an active metabolite of the synthetic antitumor agent HMN-214, restores chemosensitivity to multidrug-resistant cells by targeting the transcription factor NF-Y. Cancer Res 2003;63:6942–7.
9. Freitas S, Moore DH, Michael H, Kelley MR. Studies of apurinic/apyrimidinic endonuclease/ref-1 expression in epithelial ovarian cancer: correlations with tumor progression and platinum resistance. Clin Cancer Res 2003;9:4689–94.
10. Pengetnze Y, Steed M, Roby KF, Terranova PF, Taylor CC. Src tyrosine kinase promotes survival and resistance to chemotherapeutics in a mouse ovarian cancer cell line. Biochem Biophys Res Commun 2003;309:377–83.
11. Schmandt RE, Broaddus R, Lu KH, et al. Expression of c-ABL, c-KIT, and platelet-derived growth factor receptor-β in ovarian serous carcinoma and normal ovarian surface epithelium. Cancer 2003;98:758–64.
12. Duan Z, Duan Y, Lamendola DE, et al. Overexpression of MAGE/GAGE genes in paclitaxel/doxorubicin-resistant human cancer cell lines. Clin Cancer Res 2003;9:2778–85.
13. Schena M, Shalon D, Davis RW, Brown PO. Quantitative monitoring of gene expression patterns with a complementary DNA microarray. Science 1995;270:467–70.
14. Ono K, Tanaka T, Tsunoda T, et al. Identification by cDNA microarray of genes involved in ovarian carcinogenesis. Cancer Res 2000;60:5007–11.
15. Ishibashi Y, Hanyu N, Nakada K, et al. Profiling gene expression ratios of paired cancerous and normal tissue predicts relapse of esophageal squamous cell carcinoma. Cancer Res 2003;63:5159–64.
16. Yuza Y, Agawa M, Matsuzaki M, Yamada H, Urashima M. Gene and protein expression profiling during differentiation of neuroblastoma cells triggered by 13-*cis* retinoic acid. J Pediatr Hematol Oncol 2003;25:715–20.
17. Schaner ME, Ross DT, Ciaravino G, et al. Gene expression patterns in ovarian carcinomas. Mol Biol Cell 2003;14:4376–86.
18. Liu J, Yang G, Thompson-Lanza JA, et al. A genetically defined model for human ovarian cancer. Cancer Res 2004;64:1655–63.
19. Hibbs K, Skubitz KM, Pambuccian SE, et al. Differential gene expression in ovarian carcinoma: identification of potential biomarkers. Am J Pathol 2004;165:397–414.
20. Santin AD, Zhan F, Bellone S, et al. Discrimination between uterine serous papillary carcinomas and ovarian serous papillary tumours by gene expression profiling. Br J Cancer 2004;90:1814–24.
21. Walter-Yohrling J, Cao X, Callahan M, et al. Identification of genes expressed in malignant cells that promote invasion. Cancer Res 2003;63:8939–47.
22. Holleman A, Cheok MH, den Boer ML, et al. Gene-expression patterns in drug-resistant acute lymphoblastic leukemia cells and response to treatment. N Engl J Med 2004;351:533–42.
23. Suganuma K, Kubota T, Saikawa Y, et al. Possible chemoresistance-related genes for gastric cancer detected by cDNA microarray. Cancer Sci 2003;94:355–9.
24. Weldon CB, Scandurro AB, Rolfe KW, et al. Identification of mitogen-activated protein kinase kinase as a chemoresistant pathway in MCF-7 cells by using gene expression microarray. Surgery 2002;132:293–301.
25. Kosary CL. FIGO stage, histology, histologic grade, age and race as prognostic factors in determining survival for cancers of the female gynecological system: an analysis of 1973-87 SEER cases of cancers of the endometrium, cervix, ovary, vulva, and vagina. Semin Surg Oncol 1994;10:31–46.
26. Koyama T, Suzuki H, Imakiire A, Yanase N, Hata K, Mizuguchi J. Id3-mediated enhancement of cisplatin-induced apoptosis in a sarcoma cell line MG-63. Anticancer Res 2004;24:1519–24.
27. Kamisango K, Matsumoto T, Akamatsu K, Morikawa K, Tashiro T, Koizumi K. Antitumor activity and cellular accumulation of a new platinum complex, (−)-(R)-2-aminomethylpyrrolidine (1,1-cyclobutanedicarboxylato) platinum (II) monohydrate, in cisplatin-sensitive and -resistant murine P388 leukemia cells. Jpn J Cancer Res 1992;83:304–11.
28. Markov GG, Arion VJ. Characteristics of nuclear-ribosomal and DNA-like ribonucleic acids differentially extracted by hot-phenol fractionation. Eur J Biochem 1973;35:186–200.
29. Sedlmayr P, Blaschitz A, Wintersteiger R, et al. Localization of indoleamine 2,3-dioxygenase in human female reproductive organs and the placenta. Mol Hum Reprod 2002;8:385–91.
30. Beer DG, Kardia SL, Huang CC, et al. Gene-expression profiles predict survival of patients with lung adenocarcinoma. Nat Med 2002;8:816–24.
31. Iizuka N, Oka M, Yamada-Okabe H, et al. Oligonucleotide microarray for prediction of early intrahepatic recurrence of hepatocellular carcinoma after curative resection. Lancet 2003;361:923–9.
32. Falini B, Tiacci E, Liso A, et al. Simple diagnostic assay for hairy cell leukaemia by immunocytochemical detection of annexin A1 (ANXA1). Lancet 2004;363:1869–70.
33. Yu Y, Khan J, Khanna C, Helman L, Meltzer PS, Merlino G. Expression profiling identifies the cytoskeletal organizer ezrin and the developmental homeoprotein Six-1 as key metastatic regulators. Nat Med 2004;10:175–81.
34. Ntzani EE, Ioannidis JP. Predictive ability of DNA microarrays for cancer outcomes and correlates: an empirical assessment. Lancet 2003;362:1439–44.
35. Spentzos D, Levine DA, Ramoni MF, et al. Gene expression signature with independent prognostic significance in epithelial ovarian cancer. J Clin Oncol 2004;22:4700–10.
36. Terness P, Bauer TM, Rose L, et al. Inhibition of allogeneic T cell proliferation by indoleamine 2,3-dioxygenase-expressing dendritic cells: mediation of suppression by tryptophan metabolites. J Exp Med 2002;196:447–57.
37. Munn DH, Zhou M, Attwood JT, et al. Prevention of allogeneic fetal rejection by tryptophan catabolism. Science 1988;281:1191–3.
38. Mellor AL, Sivakumar J, Chandler P, et al. Prevention of T cell-driven complement activation and inflammation by tryptophan catabolism during pregnancy. Nat Immunol 2001;2:64–8.
39. Uyttenhove C, Pilotte L, Theate I, et al. Evidence for a tumoral immune resistance mechanism based on tryptophan degradation by indoleamine 2,3-dioxygenase. Nat Med 2003;9:1269–74.
40. Friberg M, Jennings R, Alsarraj M, et al. Indoleamine 2,3-dioxygenase contributes to tumor cell evasion of T cell-mediated rejection. Int J Cancer 2002;101:151–5.
41. Munn DH, Shafizadeh E, Attwood JT, Bondarev I, Pashine A, Mellor AL. Inhibition of T cell proliferation by macrophage tryptophan catabolism. J Exp Med 1999;189:1363–72.
42. Munn DH, Sharma MD, Lee JR, et al. Potential regulatory function of human dendritic cells expressing indoleamine 2,3-dioxygenase. Science 2002;297:1867–70.
43. Frumento G, Rotondo R, Tonetti M, et al. Tryptophan-derived catabolites are responsible for inhibition of T and natural killer cell proliferation induced by indoleamine 2,3-dioxygenase. J Exp Med 2002;196:459–68.
44. Terness P, Bauer TM, Rose L, et al. Inhibition of allogeneic T cell proliferation by indoleamine 2,3-dioxygenase-expressing dendritic cells: mediation of suppression by tryptophan metabolites. J Exp Med 2002;196:447–57.
45. Ishio T, Goto S, Tahara K, Tone S, Kawano K, Kitano S. Immunoactivative role of indoleamine 2,3-dioxygenase in human hepatocellular carcinoma. J Gastroenterol Hepatol 2004;19:319–26.
46. Oh GS, Pae HO, Choi BM, et al. 3-Hydroxyanthranilic acid, one of metabolites of tryptophan via indoleamine 2,3-dioxygenase pathway, suppresses inducible nitric oxide synthase expression by enhancing heme oxygenase-1 expression. Biochem Biophys Res Commun 2004;320:1156–62.
47. Matthews NE, Adams MA, Maxwell LR, Gofton TE, Graham CH. Nitric oxide-mediated regulation of chemosensitivity in cancer cells. J Natl Cancer Inst 2001;93:1879–85.
48. Postovit LM, Adams MA, Lash GE, Heaton JP, Graham CH. Nitric oxide-mediated regulation of hypoxia-induced B16F10 melanoma metastasis. Int J Cancer 2004;108:47–53.
49. Wenzel U, Kuntz S, Daniel H. Nitric oxide levels in human preneoplastic colonocytes determine their susceptibility toward antineoplastic agents. Mol Pharmacol 2003;64:1494–502.
50. Muller AJ, DuHadaway JB, Donover PS, Sutanto-Ward E, Prendertgast GC. Inhibition of indoleamine 2,3-dioxygenase, an immunoregulatory target of cancer suppression gene Bin1, potentiates cancer chemotherapy. Nat Med 2005;3:312–9.
51. Nakanishi C, Toi M. Nuclear factor-κB inhibitors as sensitizers to anticancer drugs. Nat Rev Cancer 2005;5:297–309.

アパタイトファイバースキャホールドの開発と臨床応用に向けた試み

Development of Hydroxyapatite Fiber Scaffolds with Future Implication of Clinical Use

Key-words：Hydroxyapatite fiber, Scaffold, Clinical application, Tissue engineering, Posterolateral fusion

松本　守雄・森末　光・相澤　守

Morio MATSUMOTO[*1], Hikaru MORISUE[*1] and Mamoru AIZAWA[*2]

(Keio University[*1]; Meiji University[*2])

1. はじめに

整形外科領域では骨折や腫瘍摘出後などにより生じた骨欠損部への骨補填，あるいは関節固定術などの際に骨移植を行う機会が多い．特に近年の高齢化社会の到来もあり，骨移植を要する手術の頻度が増加している．骨移植時には患者の自家骨を腸骨などから採取して用いるのがスタンダードな方法であるが，採骨に伴う合併症や，十分な採骨量の確保が困難であるなどの問題点がある．特に，骨粗鬆症のある高齢者や体の小さい幼小児ではこれらの問題は切実である．そこで，骨移植材料として種々の生体活性セラミックが開発され，臨床応用されてきた．しかし，セラミック単独では，骨誘導能は期待できないことから，骨誘導を得るために生体活性セラミックを骨形成因子（human recombinant bone morphogenetic protein, rh-BMP）などの骨誘導性タンパクのキャリアとして用いる，あるいは骨細胞，増殖因子とともにスキャホールドとして tissue engineering に用いるなどの方法が試みられている．生体活性セラミックのなかでも水酸アパタイト[$Ca_{10}(PO_4)_6(OH)_2$：HAp(Ca/P=1.67)]は生体骨の無機成分と類似した組成を持ち，優れた生体適合性を有するため，生体活性物質のキャリアとして，あるいは tissue engineering のスキャホールドとして有用と考えられ，事実，実験的，臨床的に広く用いられている．

しかし，従来の水酸アパタイトが生体活性物質のキャリアとして，あるいはスキャフォールドとして最良かどうかについては疑問がある．たとえば水酸アパタイトは多孔体といえども細胞の3次元培養は困難であることや，生体活性物質のスキャフォールドとしては生体内吸収性に乏しいなどである．そこで，筆者らはこれらの問題を解決するべく，ハイドロキシアパタイトファイバーの開発を行った．

本稿では，筆者らが開発したハイドロキシアパタイトファイバースキャホールド(AFS)[1)~9)]について紹介し，その臨床応用にむけた研究について概説する．

2. AFS の作製法

均一沈殿法により長軸径 100μm のアパタイト単結晶ファイバーを合成し，それらの繊維の係合を利用して AFS を作製する．

従来のアパタイト単結晶ファイバーを敷き詰めて作製した AFS (AFS0)は，メッシュ構造をしているため高い気孔率(95%)を持つものの，マクロ孔に乏しく(平均気孔径 5μm)，細胞の内部への侵入が困難であった．そこで，AFS 内部への細胞侵入を容易にするため，成形時にカーボンビーズを用いて内部に空洞を形成した（AFS1000：気孔径 100μm，気孔率 98%，AFS2000：250μm，99%）．なお，ここで AFS2000 とはアパ

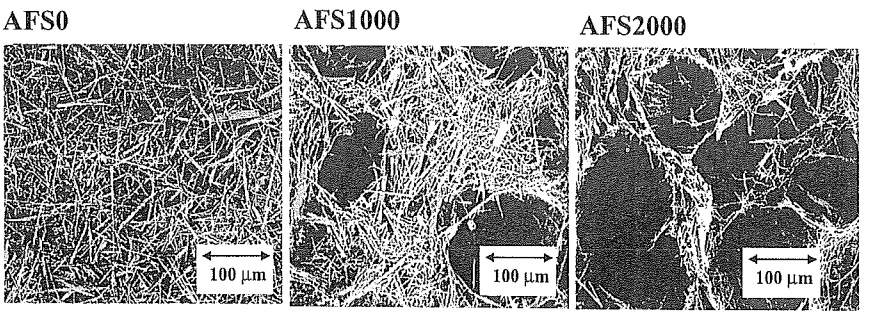

スキャホールドの作製条件と性質

試料名	Carbon/HAp [w/w]	気孔率 [%]	細孔メジアン径 [μm]
AFS0	0/1	94±0.5	5.2
AFS1000	10/1	98±0.1	112.8
AFS2000	20/1	99±0.1	247.3

多孔質セラミックスの骨侵入に必要な細孔径

100 μm以上　：石灰化骨の形成
40~100 μm　：骨様物質で埋まる中間層の形成
5 ~15 μm　：コラーゲン繊維および血球の通る気孔

図1　スキャホールドの性質およびそれらの微細構造

タイト単結晶ファイバーを1に対してカーボンビーズを質量で20倍量添加して作製したものである．これにより，AFSは内部の気孔率，平均気孔径が自在に調節可能で，細孔径の拡大と連通孔が作成可能となった（図1）．

3. *in vitro* での評価

AFSにおける細胞増殖性と分化について有効性を評価するため，マウス由来骨芽細胞様細胞であるMC3T3-E1あるいはラット骨髄間葉系幹細胞をAFS（AFS0，AFS1000，AFS2000）内に播種して培養を行い，細胞増殖度，アルカリフォスファターゼ活性およびオステオカルシン濃度の測定を行った．細胞増殖性は細胞の産生するDNA量を測定して求めた．その結果，細胞の増殖性は，AFS2000，AFS0，Control（ポリスチレンプレート）の順に良好であった．特に，他の基材と比較してAFS2000では培養期間が7日目から21日目まで順調な細胞数の増加が観察された．これは，AFS0では細胞が内部まで侵入できずに表面付近でのみ増殖していたのに対し，AFS2000では細胞が侵入するのに十分な大きさの細孔径であったために，細胞がスキャフォルドの内部にまで十分に侵入し，三次元培養が行われたためと考えられる（図2）．また，アルカリフォスファターゼ活性およびオステオカルシン濃度もAFS2000で有意に高く，AFS内で骨芽細胞様細胞への分化能が維持されていることが示唆された．

4. *in vivo* での評価

さらに，AFSを単独でラット皮下に移植した際には，移植後6週でAFSの著明な縮小が見られたことからAFSは良好な生体吸収性を有することが明らかとなった．生体親和性が高いとされる水酸アパタイトとはいえ生体にとっては異物であることから，AFSの有する良好な生体吸収性は本スキャホールドのもつ利点の一つと考えられる．

スキャホールドとしてのAFSの適性を評価するため，ラット骨芽細胞様細胞を用いてヌードマウスの皮下移植実験を行った．

1日齢ラット頭蓋骨を酵素処理して得た5×10^6個の骨芽細胞様細胞をAFS（AFS0，AFS2000）に播種し，デキサメタゾン，アスコルビン酸，βグリセロリン酸ナトリウムにより骨芽細胞への分化を誘導しつつ約2週間 *in vitro* にて三次元培養し，「再生培養骨」を作製した．4週齢ヌードマウスの背部皮下に再生培養骨を移植し，術後1，4および12週にAFSを摘出，レントゲン撮影および病理組織標本を作製し，骨形成の有無につき評価を行った．

AFS0の病理組織所見では，骨組織はAFS内部には認めず，辺縁にのみ形成された．一方，AFS2000病理組織所見では，AFSは著明に縮小しているものの，骨組織が内部に明瞭な形成を認めた（図3）．骨芽細胞のマーカーである抗ラットオステオカルシン抗体を用いた免疫染色も陽性であり，AFS内部には骨芽細胞の増生が確認された．

本結果は背部皮下という骨芽細胞の存在しない生体内環境下でも再生培養骨が骨形成を行うことを示しており，再生培養骨は骨誘導能を示すことがわかった．

5. 臨床応用に向けた研究

筆者らはAFSを臨床に応用するためラットの脊椎後側方固定術モデルを作成した．脊椎後側方固定術は，不安定性のある腰椎疾患などにしばしば行われる手術であるが，腰椎の後外側に骨移植を行い，腰椎を骨性に癒合させ，安定化させる術式である[10]．

Bone morphogenetic protein（BMP）のcarrierとしてすでにコラーゲンシートや既存の水酸アパタイトなどが臨床応用されているが，骨癒合に多量のBMPを要するなどの問題があった[11]．そこで本研究ではAFSをBMPのキャリアとして用い，骨癒合の有無を判定し，その有用性を評価した．

移植実験に先立ち，AFSのBMP放出能（releasing efficiency）に関する *in vitro* 実験を行った．Rh-BMP2（アステ

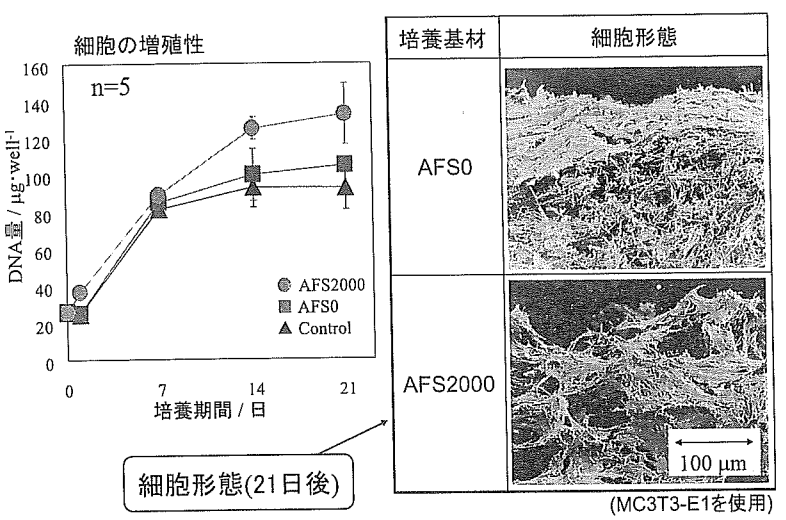

図2　スキャホールドに播種した細胞の増殖性と形態

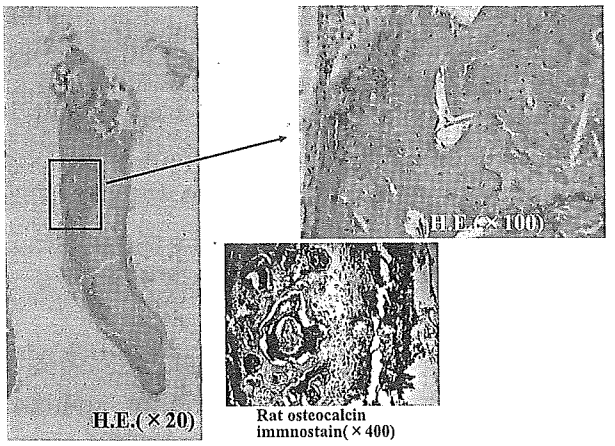

図3　再生培養骨インプラント12週後の組織学的所見
（HE，OC免疫染色；AFS2000）

ラス製薬（旧，山之内製薬）より供与）をAFSおよび市販の水酸アパタイトブロック（Apaceram，Pentax Inc. Tokyo Japan；気孔率55%，気孔径約100μm，5mm×6mm×1mm大）に吸収させた後，PBS中に浸した．28日間にわたり，PBS中に放出されたrh-BMP2の合計量をenzyme linked immunoassay法により計測した．その結果，AFSでは浸透24時間後にrh-BMP2の約40%が放出され，総放出量は28日後まで徐々に増加し，最終的には50%が放出された．これに対し，市販の水酸アパタイトブロックでは総放出量は6%に過ぎなかった．このような結果から，AFSは良好なBMP放出能を有することが明らかとなった．

移植実験には，直径約12mm，高さ3mm（0.34cm^3）の円柱形に作製したAFSを使用した．比較対照として，前述の既存水酸アパタイトブロックを14mm×4mm×4mmの直方体に加工して使用した．これらのアパタイトに同一の量のrhBMP-2（5または10μg）を含ませて移植に用いた．

14週齢Wister rat（脊椎固定術モデル）に対して，第5～6腰椎間両側に後側方固定術を行い，移植後28および56日目に第5～6脊椎を一塊として摘出した．骨癒合の有無を徒手検査，ソフテックス，μCTによる画像解析および病理組織学的検査により評価し，両群間で比較検討した（図4）．

徒手検査の結果では，BMP10μg投与では，AFS群，比較対象のブロック群も術後4週および8週時において70～100%と高い骨癒合率を得ていた．しかしながら，5μg投与では，AFS1000使用群においてのみ術後4週目で100%，術後8週目で88%と，10μg負荷時と同様に高い骨癒合率が得られた．AFS0群，AFS2000群はAFS1000群と比べて低い骨癒合率であったが，最も骨癒合率が低かったのはブロック群であり，術後4週目の骨癒合率が0%，術後8週目が33%となった．

ソフテックス像では，AFS群では，第5～6腰椎側方に新生骨形成を旺盛に認め，腰椎が強固に架橋されていた（図5a）．一方，ブロック群は，セラミックスからやや離れた位置に形成された新生骨が腰椎から外側に広がっていた．また，μCT像では，術後4週で，AFS群では，脊椎に密着したシートを中心に旺盛な骨形成が得られたのに対し，ブロック群では，脊椎からやや離れた位置に，セラミックを囲むように骨が形成された（図5b）．骨の内部には空洞形成が目立った．さらに，AFS1000群とブロック群のμCT像をコンピューター解析によって骨形成の程度につき詳しく計測すると，AFS群ではブロック群と比較して，骨梁形成が有意に多かった．

病理所見ではAFS周囲のみならず内部にも良好な骨梁形成が術後4週の段階で確認された．一方，ブロックでは骨形成は認めるものの，ブロック内部の骨形成は明らかではなく，ブロックと周囲に形成された骨の間には線維性組織が介在していた．

以上の結果から，AFSは既存のハイドロキシアパタイトブロックと比較してより高い骨癒合率および高密度の骨形成が得られることから腰椎後側方固定術におけるrh-BMP2の有望なキャリアであると考えられる．

6. おわりに

臨床応用可能なスキャホールドの備える条件として，①生体と類似した環境を与えること（三次元培養が可能なこと），②細胞の活性を維持および促進すること（細胞の分化誘導），③移植部位に応じた十分な力学的強度を有すること（たとえば荷重部位では高い

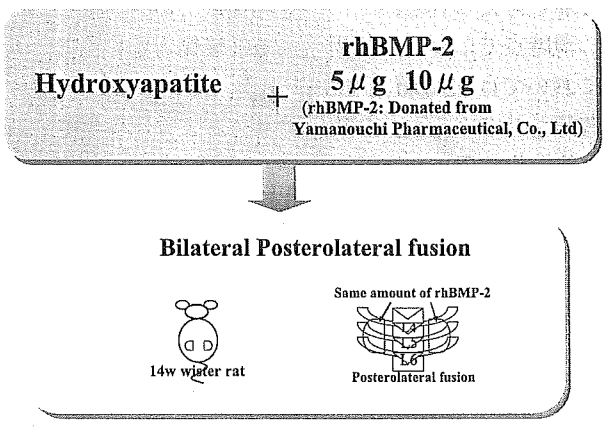

図4　ラット腰椎後側方固定術モデル

a. ソフテックス像

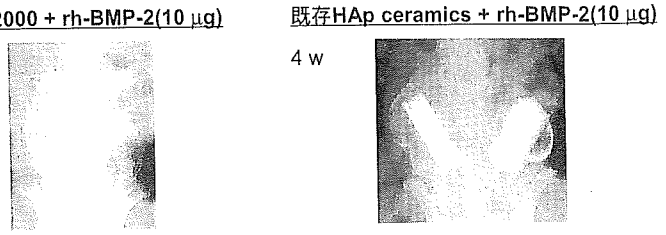

b. μCT像

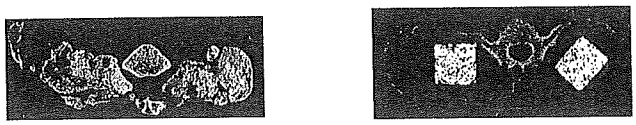

図5　ラット腰椎後側方固定術モデルにおけるソフテックス像およびμCT像（術後4週）

力学的強度が必要とされる）および④ホストの組織と置換すること（生体吸収性）が求められている．実際，コラーゲンスポンジのような生体由来材料やポリ乳酸（PLA），ポリグリコール酸（PGA）およびそれらの共重合体（PLA/PGA）などの生分解性ポリマー，そして水酸アパタイト（$Ca_{10}(PO_4)_6(OH)_2$；HAp）やβ-リン酸三カルシウム（β-$Ca_3(PO_4)_2$；β-TCP）のような多くの素材がスキャホールドとして実験的あるいは実際の臨床の場で用いられている．しかし，これらのスキャホールドは必ずしも上記の4つの条件をすべて満たしてはいるとはいえない．

AFSは*in vitro*で旺盛な細胞付着，分化および増殖能を呈し，*in vivo*ではAFS内培養細胞は内軟骨性骨化を呈した．また，腰椎後側方固定術モデルでは良好な骨癒合が得られた．このように，AFSは骨再生のスキャホールドとして，あるいは骨誘導性タンパクのキャリアーとして，その有用性が期待できる．問題点としては，力学的強度に劣ることが挙げられるが，コラーゲンの添加などの改良を加えることにより，克服可能と考えられる．

現時点ではラットを用いた脊椎後側方固定術モデルにおいてはrh-BMP2のキャリアーとしての有用性が確認されているが，今後は骨癒合がより困難とされる高等動物を用いた実験が必要である．また，実際のヒトへの応用時には大量のrh-BMP2が必要とされ，医療経済上の問題を生じることも考えられることから[12]，tissue engineeringにより*in vitro*で構築した再生骨を移植に用いる研究も進めてゆく予定である．

文　献

1) M. Aizawa, H. Shinoda, H. Uchida, K. Itatani, I. Okada, M. Matsumoto, H. Morisue, H. Matsumoto and Y. Toyama, *Key Engineer Materials*, 240-242, 647-50 (2003).
2) 相澤　守，伊藤まどか，板谷清司，岡田　勲，松本守雄，*Phosphorus Letter*, 46, 7-14 (2003).
3) M. Aizawa, H. Shinoda, H. Uchida, K. Itatani, I. Okada, M. Matsumoto, H. Morisue, H. Matsumoto and Y. Toyama, *Key Engineer Materials*, 240-242, 647-50 (2003).
4) M. Aizawa, H. Shinoda, H. Uchida, I. Okada, J. Fujimi, N. Kanzawa, H. Morisue, M. Matsumoto and Y. Toyama, *Phosphorus Res Bull*, 17, 268-273 (2004).
5) 相澤　守，篠田洋紀，松本守雄，*Phosphorus Letter*, 51, 3-12 (2004).
6) 相澤　守，松本守雄，遺伝子医学別冊 BioMedical Quick Review Net, No.402 (2004).
7) M. Aizawa, A.E. Porter, S.M. Best and W. Bonfield, *Biomaterials*, 26, 3427-33 (2005).
8) 松本守雄，千葉一裕，戸山芳昭，相澤　守，骨・関節・靱帯，16, 239-45 (2003).
9) 森末　光，松本守雄，戸山芳昭，相澤　守，整形外科，55, 1672 (2004).
10) SD. Boden, J. Kang, H. Sandhu and JG. Heller, *Spine*, 27, 2662-73 (2002).
11) SD. Boden, *Spine*, 27, S26-31 (2002).
12) H. Ohgushi and AI. Caplan, *J Biomed Mater. Res.*, 48, 913-27 (1999).

筆者紹介

松本　守雄（まつもと　もりお）
1986年，慶應義塾大学医学部卒業．同大学整形外科助手．2003年4月より同大学整形外科専任講師．2005年4月より同大学運動器機能再建・再生学講座助教授．専門領域　脊椎・脊髄外科学，生体材料学．
[連絡先]　〒160-8582　東京都新宿区信濃町35　慶應義塾大学医学部　ユニデン寄付講座　運動器機能再建・再生学
E-mail：morio@sc.itc.keio.ac.jp

森末　光（もりすえ　ひかる）
1995年，慈恵医科大学卒業．慶應義塾大学整形外科助手．専門領域：脊椎・脊髄外科学，生体材料学

相澤　守（あいざわ　まもる）
1992年上智大学大学院理工学研究科博士前期課程修了，1992年花王(株)素材研究所勤務，1993年上智大学理工学部助手（2001年10月～2002年9月英国ケンブリッジ大学　客員研究員），2003年より現職．専門：バイオマテリアル・セラミックス・組織工学．
[連絡先]　〒204-8571　川崎市多摩区東三田1-1-1　明治大学理工学部工業化学科
E-mail：mamorua@isc.meiji.ac.jp

多孔質水酸アパタイトを用いたバイオ人工肝臓

Bioartificial Liver Filled Up a Cylindrical Module with Porous Hydroxyapataite Beads

Key-words：Bioreactor, Scaffold, Liver

松浦　知和・幡場　良明・石川　周太郎・小川　哲朗

Tomokazu MATSUURA[*1], Yoshiaki HATABA[*1], Syutaro ISHIKAWA[*2] and Tetsuro OGAWA[*3]

([*1]The Jikei University School of Medicine, [*2]Biott Co., Ltd., [*3]PENTAX Corp.)

1. はじめに

バイオ人工肝臓の臨床における用途は，肝不全患者の加療であり，体外循環型バイオ人工肝臓と体内埋め込み型バイオ人工肝臓の開発が必要とされている．前者は，肝臓移植待機患者の全身状態の維持・管理や，急性肝不全患者の救命に必要である．また，後者は，非代償性肝硬変から慢性肝不全で意識障害などを繰り返す患者の quality of life (QOL)の向上に開発が望まれている．さらに，外傷性ショックや肝障害患者においてはアルブミンなどの血漿製剤の補充が必要であるが，バイオ人工肝臓は安全で安価な血漿製剤の生産系としても応用できる可能性がある．

筆者らがバイオ人工肝臓本体として用いているラジアルフロー型バイオリアクター (radial-flow bioreactor：RFB) は，筒状のリアクターに細胞培養担体をスキャホールドとして充填した細胞充填型バイオリアクターである (図1)[1]．本リアクターは培養液を筒の周囲から中心にむかって還流することにより，高密度培養によって生じる供給酸素・栄養素の偏向を軽減することができるように，設計されている．充填する担体としては，硬質素材として多孔質ガラスビーズ Siran (Schott, Maintz, Germany)) が用いられてきたが，現在製造中止となっている[2]．筆者らは，医療用素材としてはガラスでは血液との接触によってブラジキニンの発生など問題が生じる可能性を考え，組織適合性が良好な水酸アパタイト (HAp) ビーズに着目し，細胞培養担体として用いてきた．

2. 多孔質ハイドロキシアパタイトビーズ

筆者らがペンタックス社と共同で開発した HAp ビーズは，粒径約 1mm で，200μm 前後の孔が開いた多孔質ビーズである．HAp は高純度のリン酸と水酸化カルシウムを水溶液中で反応させて合成した．得られた沈殿を乾燥させた後，再び懸濁し，そのスラリーを撹拌・発泡させて乾燥ブロックを得た．HAp の多孔質構造は，スラリーの発泡状態を気泡剤および撹拌条件を制御することで調整した．これを大きさ 1～2mm の大きさを持つ顆粒状に加工後，1200℃にて焼結させて，HAp 多孔体とした．多孔体を粉砕・分級することにより，HAp 多孔質ビーズを作成した．有孔率は 50～90%で，孔内にも細胞が付着培養できる構造を有している (図2)．気孔率 50%の担体は 1～10μm と数十～数百 μm の 2 種類の気孔を持つ多孔体

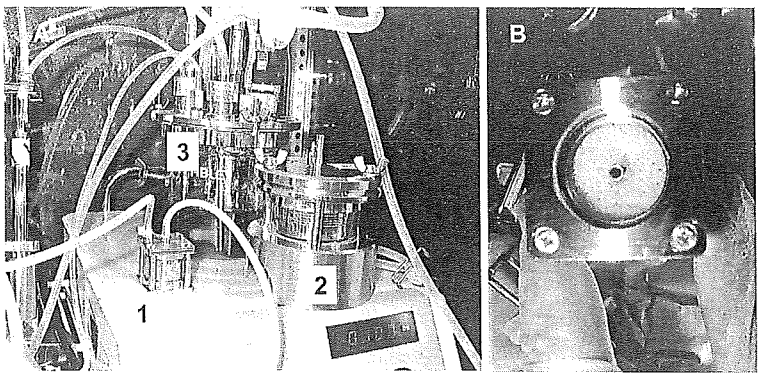

図1　A；ラジアルフロー型バイオリアクター (RFB)．5ml 容量 RFB (1)，15m*l* 容量 RFB (2)，リザーバー (3)．リザーバー内の培養液はポンプによって RFB に還流される．15m*l* 容量の RFB はブタ体外循環実験に用いた．B；5m*l* 容量の RFB 内にハイドロキシアパタイト担体を充填したところ．培養液は円筒の周囲より中心部に向けて還流される

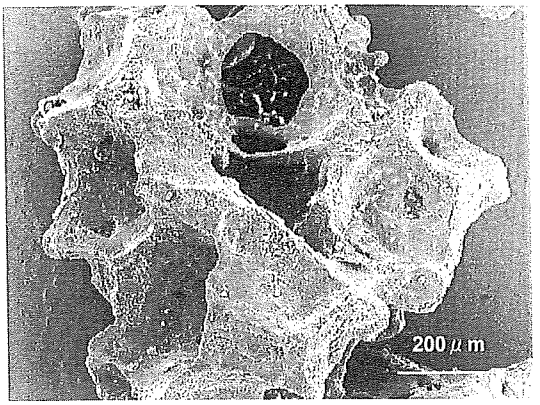

図2　ハイドロキシアパタイト（HAp）ビーズ．有孔率50～80%程度のHApビーズで，細胞が表面および内腔面一面に生着している

であり，大きな気孔は小さな気孔と連通していた．また，気孔率90%の多孔体は数百 μm の気孔が直接連通した構造であった．こうした培養担体はリアクターのスケールアップには有用であると考える．なぜなら，セルロースビーズやコラーゲンビーズではスケールアップをすると，重力でリアクターの下層の細胞培養担体が押し潰されて還流不全をまねく可能性が大きいからである．

多孔質であることは，一定の容積のバイオリアクター内での細胞付着表面積を広くし，高密度大量培養が可能となる．HApビーズは細胞付着性にもすぐれ，図2に示すビーズには，表面および内腔面一面にヒト肝臓由来細胞が培養されている．さらに，HApから有害物質の溶出はなく，生体組織・血液との組織適合性に優れ，組織からの毒性物質の誘導もほとんどない．そのため実際に1980年代以降人工骨として臨床応用されている[3]．

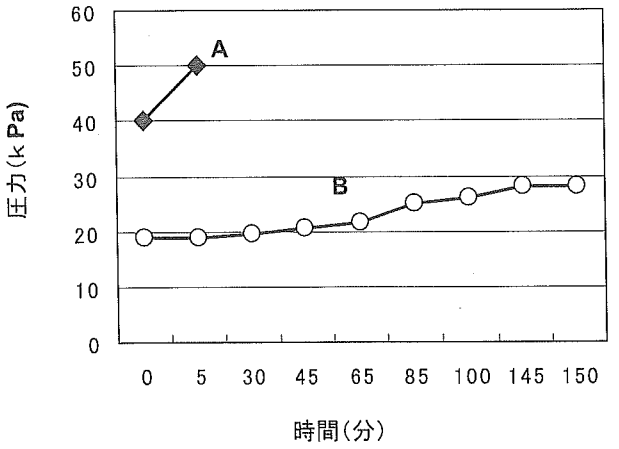

図3　水を還流したラジアルフロー型バイオリアクター（RFB）の流入部にかかる還流圧．A：HApビーズを充填し，数回還流したRFBに水を還流してみると当初より40kPaと還流圧が高く，5分間の還流で50kPaを超えて，還流不全を起こした．B：そのRFBの還流液流出部のHApビーズの破片を取り除き，新しいHApビーズを充填したところ，還流圧は20～30kPaに抑えられ，還流不全は起こらなかった

一方，体外循環型バイオ人工肝臓の実用化には，約100ml容量のバイオリアクターにHApビーズを充填し，さらに粘性が高い血漿を還流する必要がある．RFBの構造上，還流液は円筒形のリアクター周囲から中心に向かって流れるため，広い流入部から狭い流出部に還流され，還流速度が内側で上昇するとともに，還流圧も内側で高くなりやすい．このため，充填細胞培養担体や細胞の特性によっては，還流圧上昇による還流不全が生じる可能性もある．実際，当初の実験ではリアクターに繰り返しHApビーズを充填して使用したところ，還流圧が上昇し，還流不全や還流チューブが接続部ではずれてしまう現象がみられた．リアクターを分解して調べたところ，繰り返し使用したRFBの流出部に細かく砕けたHApビーズの破片が詰まっていることが判明した．この対策として，①実験前にRFBを分解して超音波洗浄器で徹底的に洗浄し破片を除き，②HApビーズもペンタックス社で洗浄し細かい破片を除いたものを用いることにした．その結果，繰り返し使用したRFBに従来のHApビーズを充填し，水を還流すると40～50kPaで還流不全を起こしていたのが，前記対策で還流圧は30kPa以下で問題なく還流することができた（図3）．

3. 体外循環型バイオ人工肝臓の構築

3.1　バイオ人工肝臓カラム

バイオ人工肝臓本体は，15ml容量のRFBに多孔質HApビーズを充填し，オートクレーブで滅菌後，RFB培養装置（エイブル社）でヒト肝細胞癌細胞FLC-4を培養した．約10日間培養後，体外循環装置にバイオ人工肝臓本体を装着した．

3.2　体外循環装置

体外循環装置は，血漿分離装置，酸素供給装置およびバイオ人工肝臓本体から構成される．動物（ブタ）の頚動脈から採取した血液は，ヘパリンが抗凝固剤として投与された後，まず血漿分離装置で血漿に分離され，血漿にはバイオ人工肝臓の細胞維持のため酸素が供給されたのちに，バイオ人工肝臓本体に還流させた．浄化された血漿は再び血球成分とともに，動物頚静脈から返血させ，6時間までの体外循環では，還流不全は起こらずスムーズに還流された．

3.3 急性肝不全モデルに対するバイオ人工肝臓の効果

キノコ毒を経門脈的に投与して惹起したブタ急性肝不全モデルに，バイオ人工肝臓補助装置を装着して体外循環を行うと，致死的な肝性脳症を回避することができた．

4. 多孔質 HAp ビーズに培養された株化ヒト肝細胞癌細胞の微細形態

株化ヒト肝細胞癌細胞 FLC-4 と FLC-5 を RFB 内で多孔質 HAp ビーズに播種したが，ともによく付着し培養された．しかし，FLC-4 は HAp ビーズの表面や内腔に単層に付着・培養されたが，FLC-5 は重層して培養された（図 4）．両細胞とも培養液の還流面には微絨毛が発達し，細胞間は強固に密着していた（図 5）．FLC-4 も単層ではあるが，細胞は正方形で立体的に培養され，細胞間は密着し，極性をもって培養された．いずれの細胞も高密度に 3 次元的に細胞は培養されたが，単層に培養される FLC-4 は，流路が増殖した細胞で塞がれることもなく，分離血漿を還流する体外循環型バイオ人工肝臓に用いるのには適した細胞であると考えられる．また，FLC-5 は重層して培養され，細胞間には毛細胆管様構造を認めた．

5. 多孔質 HAp ビーズに培養された株化ヒト肝細胞癌細胞の機能

HAp ビーズに 3 次元高密度培養された細胞の機能すべてが上昇するわけではない．しかし，外的刺激（例えば薬剤や他の細胞との共培養）によって，遺伝子発現は著しく変化する．例えば，薬物代謝第 I 相反応の主たる代謝酵素であるチトクローム P450（CYP）には，多くの分子種があるが，CYP3A4 はこの中でも臨床で用いる薬剤の約 50％の代謝にかかわる重要な分子種である．CYP3A4 は人体では種々の薬剤で誘導され，薬物相互作用を起こしうる酵素であるが，RFB で培養し抗結核薬であるリファンピシンで生体に近い CYP3A4 mRNA および酵素活性を誘導することができる[4]．したがって，HAp ビーズで細胞を高密度 3 次元培養するのみでは，バイオ人工肝臓として用いることはできない．バイオ人工肝臓の目的にそった細胞を選択し，3 次元高密度培養した時の特性を解析し，目的の機能がどのような培養条件で誘導されるか明らかにすることが重要であると考える．

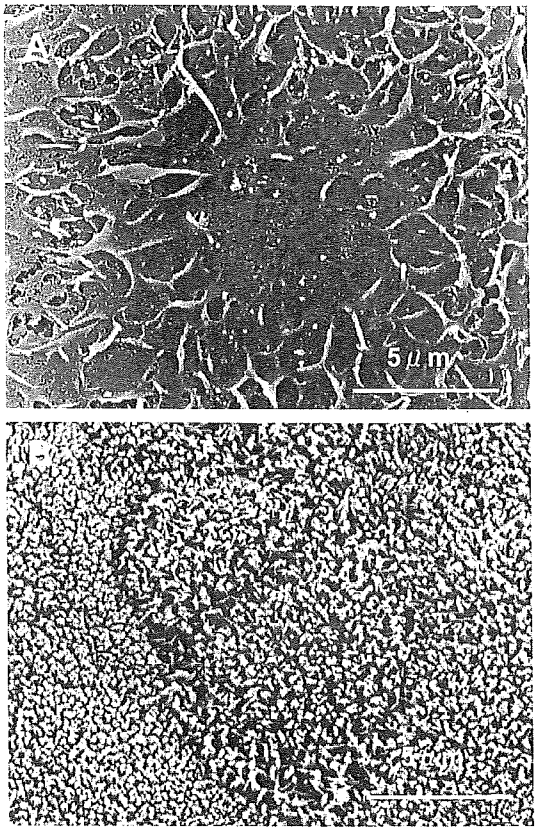

図 5　A；還流側からみた FLC-4 細胞．細胞表面にはシリア状の微絨毛が観察される．B；FLC-5 の細胞表面はさらに密に桿状の微絨毛が観察される

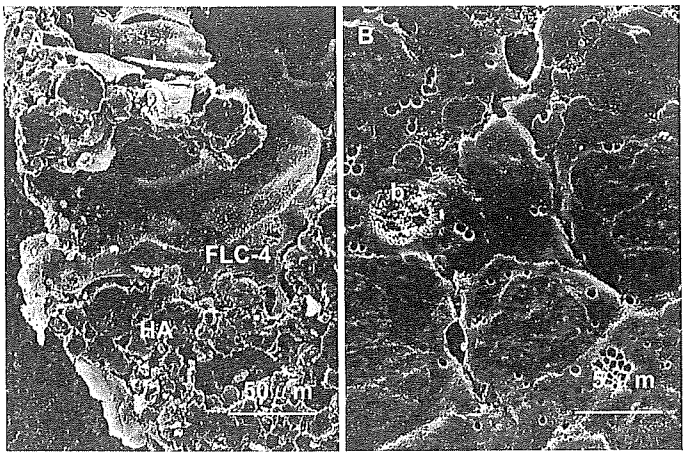

図 4　A；FLC-4 細胞は HAp ビーズに単層に培養された．しかし，細胞の還流側には微絨毛が発達しており，立体的に培養された細胞同士は密着し，極性を保って培養された．B；FLC-5 では，HAp ビーズ（HA）に重層して細胞が培養された．盲端になっているが，細胞間には毛細胆管様構造が観察された（b）

6. これから期待されること

バイオ人工肝臓の開発の方向性は，今後体外循環型バイオ人工肝臓から，生体埋め込み型バイオ人工肝臓の開発に進む必要があると

考える．このためにも，生体適合性が良く安全なHApは細胞培養担体としてとして有用である．その細胞ソースが胚性幹細胞，骨髄細胞，臍帯血細胞などを，HAp細胞付着担体を充填したRFB内で，肝細胞に分化増殖させた上で，生体に移植することができれば，肝臓移植におけるドナー不足を補い，また従来移植の適応が難しかった非代償性肝硬変患者のQOLの改善に寄与できることが期待される．

7. まとめ

多孔質HApビーズはヒト肝臓由来細胞の付着性にすぐれ，RFB内に充填し還流培養することで，高密度3次元培養を実現できた．体外循環型バイオ人工肝臓の機能発現やスケールアップにもHAp硬質ビーズは有用であった．今後，移植用臓器を生体外で作成し生体に埋め込むため，代用臓器の骨格になるHAp担体の開発に今後のニーズがあると考える．

文　献

1) M. Kawada, S. Nagamori, H. Aizaki, K. Fukaya, M. Niiya, T. Matsuura, et al., *In Vitro Cell. Dev. Biol.*, 34, 109-15 (1998).
2) T. Matsuura, M. Kawada, S. Hasumura, S. Nagamori, T. Obata, M. Yamaguchi, et al., *Int. J. Artif. Organs*, 21, 229-34 (1998).
3) 山本　晃, 中島武彦, 富永芳恵, 小川哲朗, 組織培養研究, 18, 235-44 (1999).
4) T. Iwahori, T. Matsuura, H. Maehashi, K. Sugo, M. Saito, M. Hosokawa, et al., *Hepatology*, 37, 665-73, (2003).

筆者紹介

松浦　知和（まつうら　ともかず）
1983年3月，東京慈恵会医科大学卒業．同大学消化器肝臓内科助手をへて，現在臨床検査医学講座講師．専門分野：臨床細胞生物学，肝臓内科．現在，バイオ人工肝臓の開発を推進中．
[連絡先]　〒105-8461　東京都港区西新橋3-25-8　東京慈恵会医科大学　臨床検査医学講座
E-mail：matsuurat@jikei.ac.jp

幡場　良明（はたば　よしあき）
1970年3月，早稲田大学・教育学部・理学科・生物学専修卒業．1986年東京慈恵会医科大学・附属形態研究室講師．2004年同・DNA医学研究所・分子細胞生物学研究部助教授．専門分野：細胞生物学，微細形態学．脾臓の立体微細構築に関する比較解剖学的研究，細胞・組織・臓器の三次元的微細構造の解析，樹状細胞と癌細胞の融合細胞の微細形態学的検討，バイオ人工肝臓の微細形態学的件等に関して，研究を進めている．
[連絡先]　〒105-8461　東京都港区西新橋3-25-8　東京慈恵会医科大学・DNA医学研究所・分子細胞生物学研究
E-mail：hatayo@jikei.ac.jp

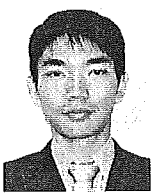

石川　周太郎（いしかわ　しゅうたろう）
東京農工大学修士卒業後，京セラで太陽電池の開発に携わる．2002年からエイブル(株)にて，培養装置の製造開発を行う．現在は，(株)バイオットにて，エイブル製の培養装置を中心に，理化学機器全般の営業を行っている．
[連絡先]　〒162-0812　東京都新宿区西五軒町6-10　(株)バイオット営業部
E-mail：shutaro@biott.co.jp

小川　哲朗（おがわ　てつろう）
1979年東京農工大学工学部工業化学科卒業，旭光工業（現，ペンタックス(株)）入社，1989年～1991年エール大学研究員を経て現職．専門：アパタイト人工骨，クロマトグラフィー．
[連絡先]　〒174-8639　東京都板橋区前野町2-36-9　ペンタックス(株)ニューセラミックス事業部開発部
E-mail：tetsuro.ogawa@aoc.pentax.co.jp

PO Box 2345, Beijing 100023, China
www.wjgnet.com
wjg@wjgnet.com

World J Gastroenterol 2006 March 28; 12(12): 1881-1888
World Journal of Gastroenterology ISSN 1007-9327

BASIC RESEARCH

Reconstruction of liver organoid using a bioreactor

Masaya Saito, Tomokazu Matsuura, Takahiro Masaki, Haruka Maehashi, Keiko Shimizu, Yoshiaki Hataba, Tohru Iwahori, Tetsuro Suzuki, Filip Braet

Masaya Saito, Division of Gastroenterology and Hepatology, Department of Internal Medicine, The Jikei University School of Medicine, Tokyo, Japan
Tomokazu Matsuura, Department of Laboratory Medicine, The Jikei University School of Medicine, Tokyo, Japan
Takahiro Masaki, Tetsuro Suzuki, Department of Virology II, National Institute of Infectious Disease, Tokyo, Japan
Haruka Maehashi, Keiko Shimizu, First Department of Biochemistry, The Jikei University School of Medicine, Tokyo, Japan
Yoshiaki Hataba, DNA Medical Institute, The Jikei University School of Medicine, Tokyo, Japan
Tohru Iwahori, Fifth Division of Blood Purification, Department of Surgery, Tokyo Medical University, Tokyo, Japan
Filip Braet, Australian Key Center for Microscopy & Microanalysis, Electron Microscope Unit, The University of Sydney, NSW 2006, Australia
Supported by grants-in-aid from the University Start-Up Creation Support System, the Promotion and Mutual Aid Corporation for Private Schools of Japan, and The Japan Health Sciences Foundation (Research on Health Sciences on Drug Innovation, KH71068).
Correspondence to: Tomokazu Matsuura, MD, PhD, Department of Laboratory Medicine, The Jikei University School of Medicine, 3-25-8 Nishi-shinbashi, Minato-ku,
Tokyo 105-8461, Japan. matsuurat@jikei.ac.jp
Telephone: +81-3-34331111 ext 3210 Fax: +81-3-34350569
Received: 2005-09-12 Accepted: 2005-10-26

Abstract

AIM: To develop the effective technology for reconstruction of a liver organ *in vitro* using a bio-artificial liver.

METHODS: We previously reported that a radial-flow bioreactor (RFB) could provide a three-dimensional high-density culture system. We presently reconstructed the liver organoid using a functional human hepatocellular carcinoma cell line (FLC-5) as hepatocytes together with mouse immortalized sinusoidal endothelial cell (SEC) line M1 and mouse immortalized hepatic stellate cell (HSC) line A7 as non parenchymal cells in the RFB. Two x 10^7 FLC-5 cells were incubated in the RFB. After 5 d, 2 x 10^7 A7 cells were added in a similar manner followed by another addition of 10^7 M1 cells 5 d later. After three days of perfusion, some cellulose beads with the adherent cells were harvested. The last incubation period included perfusion with 200 nmol/L swinholide A for 2 h and then the remaining cellulose beads along with adherent cells were harvested from the RFB. The cell morphology was observed by transmission electron microscopy (TEM) and scanning electron microscopy (SEM). To assess hepatocyte function, we compared mRNA expression for urea cycle enzymes as well as albumin synthesis by FLC-5 in monolayer cultures compared to those of single-type cultures and cocultures in the RFB.

RESULTS: By transmission electron microscopy, FLC-5, M1, and A7 were arranged in relation to the perfusion side in a liver-like organization. Structures resembling bile canaliculi were seen between FCL-5 cells. Scanning electron microscopy demonstrated fenestrae on SEC surfaces. The number of vesiculo-vacuolar organelles (VVO) and fenestrae increased when we introduced the actin-binding agent swinholide-A in the RFB for 2h. With respect to liver function, urea was found in the medium, and expression of mRNAs encoding arginosuccinate synthetase and arginase increased when the three cell types were cocultured in the RFB. However, albumin synthesis decreased.

CONCLUSION: Co-culture in the RFB system can dramatically change the structure and function of all cell types, including the functional characteristics of hepatocytes. Our system proves effective for reconstruction of a liver organoid using a bio-artificial liver.

Key words: Liver organoid; Organ reconstruction; Bio-artificial liver; Coculture; Liver sinusoidal endothelial cell; Hepatocytes; Fenestrae; Vesiculo vacuolar organelles; Radial flow bioreactor

Saito M, Matsuura T, Masaki T, Maehashi H, Shimizu K, Hataba Y, Iwahori T, Suzuki T, Braet F. Reconstruction of liver organoid using a bioreactor. *World J Gastroenterol* 2006; 12(12): 1881-1888

http://www.wjgnet.com/1007-9327/12/1881.asp

INTRODUCTION

Liver regeneration technology has made many advances in recent years. Efforts now are being made toward development of embryonic stem cells (ES cells), differentiation of hemopoietic stem cells, and development of isolation and culture methods for somatic stem cells originating from different organs. Hemopoietic stem cells, hepatoblasts originating from fetal liver, hepatocytes, and pancreatic duct epithelial cells have been included in the list of candi-

date cells for liver regeneration[1]. Development of immortalized cells by introduction of the simian virus 40 (SV40) large T antigen gene or human telomerase reverse transcriptase (hTERT) is also under investigation[2]. To date, however, no technique for regenerating and reconstructing parenchymal organs using these cells has been established. Conventional cell culture methods have achieved this goal clinically for skin, cornea, and bone tissue[3-5].

Reconstruction of organs such as the liver requires maintenance of viable cells at a high density and coculture under conditions favorable to several different cell types that constitute a liver. To make a culture system is important in reconstructing a liver organoid. Conventional stationary culture techniques are not well suited to the culture of cells in a layered form, i.e., in a structural and functional organoid a simple air/CO_2 incubator does not deliver adequate oxygen supply to layered cells. Furthermore, high-density culture cannot be maintained with the limited nutrients available in conventional cultures. For these reasons, construction of a bioreactor that allows 3-dimensional growth in a high-density perfusion culture has been advocated for reconstructing a liver organoid. In our study a radial-flow bioreactor (RFB) developed in Japan was used as a candidate model for high-density perfusion culture. Filled with a porous carrier, this bioreactor permits culture at a cell density 10 times higher than that allowed by a hollow-fiber culture system[6, 7]. Another important point is to select a cell source. In clinic, cells using bio-artificial liver are required to be highly functional and supplied quickly in large quantities. Therefore we established a functional human hepatocellular carcinoma cell line (FLC-5), which can express drug-metabolized enzymes (e.g., human-type carboxyl esterase or cytochrome) and liver-specific proteins such as albumin. *In vitro* this cell line retains its three-dimensional form, developing distinct microvilli on the surface. These cells can be cultured in serum-free ASF104 medium (Ajinomoto, Tokyo). A liver organoid cannot be reconstructed with hepatocytes only. At minimum, coculture of hepatocytes with nonparenchymal cells, such as sinusoidal endothelial cell (SEC) and hepatic stellate cell (HSC) is required. So we established immortalized SEC line M1[8] and an immortalized HSC line A7[9] by isolating nonparenchymal cells from an H-2Kb-tsA58-transgenic mouse liver transfected with the SV40 large T antigen gene[10].

Reconstruction of the liver sinusoid is important for activity of the liver organoid as a functional unit. Also, the open pores on the surfaces of SEC in fenestrae have an important functional role in the liver sinusoid. Fenestrae are the most remarkable characteristics of SEC, as first described by Wisse in 1970[11] using transmission electron microscopy (TEM). Diameters of these pores vary between species, ranging from 100 to 200 nm[12]. These fenestrae facilitate the transport of materials and solutes from the luminal to the abluminal side of the liver parenchymal cells and *vice versa*[13]. The process and mechanism of formation of these pores remain largely unclarified[14, 15]. The presence of actin filaments at the margin of these pores has been demonstrated by electron microscopic studies[16, 17]. Swinholide A, a most potent microfilament-disrupting drug available, has been demonstrated to increase the number of SEC fenestrae[14]. However, when immortalized SEC was treated in a monolayer culture or as a monoculture in the RFB, an increase in number of fenestrae could not be observed when the Swinholide A was introduced. The potential for drug-induced increase also has been reported to disappear in long-term cultures[8].

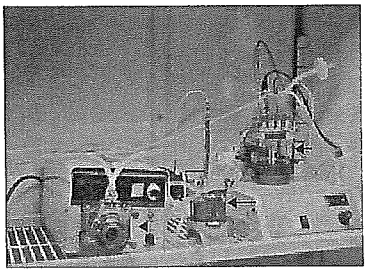

Figure 1 The system of radial-flow bioreactor. A 15-mL radial-flow bioreactor (large arrow), a mass flow controller (arrow head), and a reservoir (small arrow) are connected each other. Culture medium is perfused in the RFB. Medium conditions (PH, oxygen, CO_2 and temperature) are controlled by computer.

In developing a high functioning organoid using a bio-artificial liver, the function, form and reactivity of pharmacological agent should be near *in vivo*. In the present study, we reconstructed a functional liver organoid using immortalized cell lines in the RFB.

MATERIALS AND METHODS

Cell culture and medium

We used the three cell lines mentioned above, FLC-5, M1, and A7. As reported, culture of M1 cells was possible in serum-free conditions while supplementation of ASF104 medium with 2% fetal bovine serum (FBS) was required for culture of A7 cells. Therefore, in coculture experiments, ASF104 medium was enriched with 2% FBS.

Coculture in radial-flow bioreactor

As reported elsewhere, the RFB system is composed of a 15-mL radial-flow chamber (RA-15; ABLE, Tokyo), a mass flow controller (RAD925, ABLE), a reservoir (Figure 1), a computer, and a tissue incubator as described previously[18] (Figure 1). The culture medium was oxygenated within the reservoir, and the pH was adjusted automatically to 7.4. Oxygen pressure in the culture medium was measured both within the reservoir and at the outlet of the bioreactor. Relative oxygen consumption was monitored on the basis of the oxygen pressure gradient. During the study the temperature within the reservoir was kept constantly at 37 ℃. Two $\times 10^7$ FLC-5 cells were inoculated into the reservoir. The bioreactor was perfused in a closed circuit for 2 h to aid cells in adhering to the porous carrier cellulose beads (Asahi Kasei, Tokyo). Subsequently the bioreactor was switched to the open-circuit mode, and incubation was continued with addition of fresh culture medium to the reservoir. After 5 d, 2×10^7 A7 cells were added in a similar manner followed by another addition of 10^7 M1 cells 5 d later. Retinol (10^{-6}mol/L) was added during the first 2 d. After three days of perfusion cellulose beads with the adherent cells were harvested, and cells deposited at the bottom of the bioreactor also were recovered. Beads with attached cells were fixed in 1.2% or 2.0% glutaraldehyde as described below.

Swinholide A experiments

We cultured the three cell lines as described above. The

last incubation included perfusion with 200 nmol/L swinholide A (Sigma catalog number S9810; S) for 2 h. The cellulose beads along with adherent cells were harvested from the bioreactor. Beads with attached cells were fixed in glutaraldehyde and prepared for morphologic observation as follows.

Electron microscopy

For scanning electron microscopy (SEM), cultured cells were fixed with 1.2% glutaraldehyde in 0.1 mol/L phosphate buffer (PB) at pH 7.4 and postfixed with 1% OsO_4 in 0.1mol/L PB. The fixed cells were rinsed twice with PBS, subsequently dehydrated in ascending concentrations of ethanol, critical point-dried using carbon dioxide, and coated by vacuum- evaporated carbon and ion-spattered gold. Specimens were observed under JSM-35 scanning electron microscope (JEOL, Tokyo) at an accelerated voltage of 10 kV.

For transmission electron microscopy (TEM), cultured cells were fixed with 2.0% glutaraldehyde in 0.1mol/L PB for 1 h and postfixed with 1% OsO_4 in 0.1mol/L PB for 1 h at 4 ℃. Specimens were dehydrated in ethanol and subsequently embedded in a mixture of Epon-Araldite. Thin sections (60 nm) were cut with a diamond knife mounted on an LKB ultratome, and stained with aqueous uranyl acetate. Specimens were examined under a JEOL 1200EX electron microscope.

Amino acid analysis of supernatants

For analysis of amino acid fractions by high-performance liquid chromatography (HPLC), supernatants were collected from FLC-5 alone and from cocultures of the three cell types in the bioreactor. Supernatants were mixed with 5% sulfosalicylic acid and allowed to stand at 4 ℃ for 15 min. After centrifugation to precipitate protein, supernatants were injected into amino acid analysis columns (L-8500, Hitachi, Tokyo).

Quantitative TaqMan RT-PCR

We measured mRNA expression for the urea cycle enzymes, carbamoyl phosphate synthetase (CPS1), ornithine carbamoyltransferase (OCT), argininosuccinatesynthetase (ASS), argininosuccinatelyase (ASL), and arginase (ARG), as well as mRNA expression for albumin, hepatocyte nuclear factor (HNF)-1 and HNF-4, by quantitative TaqMan reverse transcription polymerase chain reaction (RT-PCR). RT-PCR was performed on the ABI PRISM 7700 sequence detection system using random hexamers from TaqMan reverse transcription reagents and the RT reaction mix (Applied Biosystems, Rockville, M) to reverse-transcribe RNA. TaqMan universal PCR Master Mix and Assays-on-Demand gene expression probes (Applied Biosystems) were used for PCR. A standard curve for serial dilution of 18S rRNAs was generated similarly. A relative standard curve method (Applied Biosystems) was used to calculate the amplification difference in urea cycle-related enzymes between cocultured and control cells, and elongation factor 1 (EF1), for each primer set and between albumin, HNF-1, HNF-4, and glyceraldehyde-3-phosphate dehydrogenase (GAPDH). Specificity was evaluated using GAPDH mRNA as an internal control (4310884E; Perkin-Elmer Applied Biosystems). Each amplification was performed in triplicate, and averages were obtained.

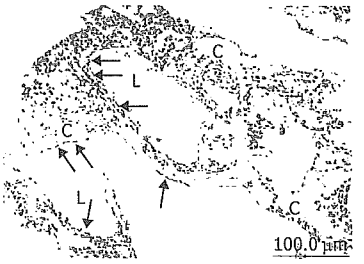

Figure 2 Light microscopic image of coculture in the RFB. High-density and layered cells attached on the cellulose beads (C). Sinusoid-like lumen structure (L) could be observed. SEC was observed with flat shape on surface of the lumen and perfusion side (arrow).

Based on DNA sequences in GenBank, primers and the TaqMan probe for albumin, HNF-1, and HNF-4 were designed using the primer design software Primer Express TM (Perkin-Elmer Applied Biosystems, Foster City, CA). AmpliTaq DNA polymerase extended the primer and displaced the TaqMan probe through its 5'-3' exonuclease activity. Probes were labeled with a reporter fluorescent dye either 6-carboxy-fluorescein (FAM) or 2, 7 dimethoxy-4,5-dichloro-6-carboxy-fluorescein (JOE) at the 5' end and a quencher fluorescent dye [6-carboxytetramethyl-rhodamine (TAMRA)] at the 3' end.

Primers/probes were as follows: ornithine transcarbamoylase (OTC) forward primer 5'-CCAGGCAATAAAAGAGTCAGGATT-3', reverse primer/ 5'-TTATCAAAG TCCCCTGGTTAGAGATACT-3', probe/ 5'-(FAM)- TTCAAATGCTCCTACACCCTGCCCTG-(TAMRA)-3'; arginosuccinase (ASL) forward primer/ 5'-TGGCCAAGGAGGTCGTCA-3', reverse primer 5'-TTCCTCGTCGTCCGGAAG-3', probe 5'-(FAM)-TGTCTTCCAGACCCGGAGACCGAA-(TAMRA)-3'; albumin forward primer/ 5'-CGATTTTCTTTTTAGGGCAGTAGC-3', reverse primer/ 5'-TGGAAACTTCTGCAAACTCAGC-3', probe/ 5'-(FAM)-CGCCTGAGCCAGAGATTTCCCA-(TAMRA)-3'; HNF-1 forward primer/ 5'-AGCGGGAGGTGGTCGATAC-3', reverse primer/ 5'-CATGGGAGTGCCCTTGTTG-3', probe/ 5'-(FAM)-TCAACCAGTCCCACCTGTCCCAACA-(TAMRA)-3'; HNF-4 forward primer/ 5'-GGTGTCCATACGCATCCTTGA-3', reverse primer/ 5'-TGGCTTTGAGGTAGGCATACTCA-3', probe/ 5'-(FAM)-CCTTCCAGGAGCTGCAGATCGATGAC-(TAMRA)-3'; GAPDH forward primer/ 5'-CTCCCCACACACATGCACTTA-3', reverse primer/ 5'-CCTAGTCCCAGGGCTTTGATT-3', probe/ 5'-(VIC)-AAAAGAGCTAGGAAGGACAGGCAACTTGGC-(TAMRA)-3'.

RESULTS

Structure of cells cultured in bioreactor

In the bioreactor, cells cultured in high density assumed layered form on the cellulose beads. Lumen-like structure was observed. Endothelial cells were exits with flat shape at the surface of the lumen and the perfusion side (Figure 2). Multiple layers of FLC-5 cells adhered to the cellulose beads, while A7 and M1 cells were predominantly localized to the side where perfusion occurred. Layered cells were seen in a hole of porous cellulose beads. Sinusoid-like lumen was observed at perfusion side in the cellulose beads